Doping dependence of normal- and superconducting-state transport properties of $Nd_{2-x}Ce_xCuO_{4\pm y}$ thin films

F. Gollnik
Lehrstuhl Experimentalphysik II, Universität Tübingen, Auf der Morgenstelle 14, 72076 Tübingen, Germany

M. Naito
NTT Basic Research Laboratories, 3-1 Morinosato-Wakamiya, Atsugi-shi, Kanagawa, 243-01, Japan
(Received 14 May 1998)

The electric and thermomagnetic transport properties of an underdoped, an optimally doped, and an overdoped *c*-axis oriented, epitaxial $Nd_{2-x}Ce_xCuO_{4\pm y}$ thin film have been investigated in the temperature range from 4.2 K to 300 K and in magnetic fields up to 11 T oriented perpendicular to the CuO_2 planes. In the normal state, the resistivity ρ, Hall coefficient R_H, and magnetoresistivity $\Delta\rho/\rho(B)$ can be described quantitatively within a simple two-carrier model if the existence of an electronlike and a holelike band is assumed, where each of the two groups of charge carriers is characterized by a temperature-independent Hall coefficient. A corresponding analysis of the thermoelectric effects appears to be more difficult since they depend on more subtle details of the band structure and the scattering mechanisms. In the superconducting regime, the critical field $B_\rho^*(T)$ determined from the shift of the resistive transition in an external magnetic field exhibits a positive curvature. In contrast, an analysis of the fluctuation conductivity and the transport entropy of magnetic flux line S_ϕ consistently gives higher values for the upper critical field $B_{c2}(T)$. The fluctuation conductivity clearly exhibits two-dimensional scaling behavior, indicating that the quasi-two-dimensional nature of the single-layer compound $Nd_{2-x}Ce_xCuO_{4\pm y}$ might be responsible for the difference between $B_\rho^*(T)$ and $B_{c2}(T)$. The order of magnitude of S_ϕ is consistent with the predictions of the Ginzburg-Landau theory. We derived material parameters as $B_{c2}(0)$, the in-plane coherence length $\xi_{ab}(0)$, the Ginzburg-Landau parameter κ, and the London penetration depth $\lambda(0)$. We also present experimental data on the Hall effect in the mixed state. [S0163-1829(98)00341-5]

I. INTRODUCTION

New questions but also new hopes for a better understanding of the high-temperature superconductors (HTSC's) were raised by the discovery of a new family of cuprates characterized by the composition $R_{2-x}Ce_xCuO_{4\pm y}$ (R = Nd,Pr,Sm,Eu).[1,2] The substitution of the trivalent rare-earth element R by Ce (presumable valence 4) suggested that electron doping of the CuO_2 planes is necessary to change R_2CuO_4 into a superconducting compound. Therefore, this class of HTSC's is usually referred to as the electron-doped or *n*-type cuprates in contrast to the majority of *p*-type HTSC's. The superconducting as well as the normal-state transport properties of the electron-doped cuprates are very different from those of *p*-type materials as $YBa_2Cu_3O_{7-\delta}$. Quantities such as the penetration depth and the surface resistance of optimally doped $Nd_{1.85}Ce_{0.15}CuO_{4\pm y}$ ($T_c \approx 24$ K) seem to exhibit BCS-like temperature dependences for small T and therefore favor *s*-wave pairing in this material.[3,4] Phase sensitive tests of the pairing symmetry in $Nd_{2-x}Ce_xCuO_{4\pm y}$ (NCCO) (to our knowledge) have not yet been reported probably due to difficulties in preparing superconducting grain boundary junctions for this material. In the normal state the resistivity of NCCO exhibits a quadratic dependence on temperature. For optimally doped samples, the Hall coefficient R_H and the thermopower S are negative with complex T dependences. The magnetoresistivity $\Delta\rho/\rho(B)$ and the Nernst effect are very pronounced. Furthermore, with increasing electron doping a sign change from negative to positive can be observed for R_H as well as for S (compare Sec. IV).

Still, we do not know if the phenomenon of superconductivity in *p*-type and *n*-type HTSC's can be understood within a common scheme. From this background evolved the intention to perform a detailed analysis of an extended set of transport coefficients in the normal as well as in the superconducting state for a series of high-quality $Nd_{2-x}Ce_xCuO_{4\pm y}$ thin films of different doping. In the following section we will describe the samples under investigation whereas Sec. III summarizes the experimental setup. The experimental results for the normal-state properties and their discussion are given in Sec. IV. Correspondingly, Sec. V deals with the superconducting state of the NCCO thin films, followed by a summary (Sec. VI).

II. SAMPLES

The intention of our experiments was to perform a doping-dependent study of the normal- and superconducting-state transport properties of $Nd_{2-x}Ce_xCuO_{4\pm y}$ thin films. Here, we have to distinguish the effects of changing the Ce content on the one hand and the oxygen content on the other hand. It is widely believed that the Ce substitution for Nd introduces additional electrons into the CuO_2 planes. Therefore, this class of cuprates is referred to as the electron doped HTSC's. [Some authors argued that an increase of the Ce fraction in NCCO might lead to an effective hole doping of

the CuO_2 planes. We do not take this standpoint since angle-resolved photoemission spectroscopy (ARPES) measurements indicate that an increasing Ce content results in a progressive filling of the Brillouin zone.[5]] The oxygen content plays a somewhat different role. After the deposition process, thin films apparently contain interstitial oxygen, which has to be removed in order to obtain optimal superconducting properties. Further reduction leaves an increasing number of oxygen vacancies and finally leads to a decomposition of the material. Nevertheless, a reversible variation of the oxygen content seems to be possible in a certain range from the underreduced to the overreduced regime.[6,7] There is a remarkable resemblance between the temperature-dependent resistivities $\rho(T)$ of under-reduced $Nd_{1.85}Ce_{0.15}CuO_{4\pm y}$ samples and underdoped $Nd_{2-x}Ce_xCuO_{4\pm y}$ samples ($x<0.15$, optimal oxygen content) as can be seen by comparison of Fig. 1(a) in Ref. 6 and Fig. 6 in Ref. 8. This might be interpreted as an indication that removing oxygen also leads to electron doping of the CuO_2-planes in NCCO. (The discussion of our experimental data will give further evidence for this interpretation.) In contrast, there are more pronounced differences between the resistivities of overreduced $Nd_{1.85}Ce_{0.15}CuO_{4\pm y}$ samples [see Fig. 1(b) in Ref. 6] and overdoped $Nd_{2-x}Ce_xCuO_{4\pm y}$ samples ($x>0.15$, optimal oxygen content; see Fig. 6 in Ref. 8). Whereas the resistivity decreases with progressive Ce doping, it increases rapidly with further oxygen reduction. The latter observation might be partly ascribed to the disorder introduced by additional oxygen vacancies.

In this paper we report on measurements on three epitaxial, *c* axis oriented NCCO thin films. They were grown by molecular-beam epitaxy on $SrTiO_3$ substrates. The thickness of the films was 90–100 nm. Details of the growth process and the microstructure of the samples can be found in Refs. 8 and 9.

Optimally doped sample (E96-353). This oxygen-reduced $Nd_{1.85}Ce_{0.15}CuO_{4\pm y}$ thin film had on optimum Ce and oxygen content with respect to a maximum critical temperature that was found to be $T_c \approx 24$ K. The sample showed resistivities of $\rho(30\ \mathrm{K}) \approx 26\ \mu\Omega\,\mathrm{cm}$ and $\rho(300\ \mathrm{K}) \approx 210\ \mu\Omega\,\mathrm{cm}$.

Underdoped sample (E95-458). In comparison with the optimally doped sample this $Nd_{1.85}Ce_{0.15}CuO_{4\pm y}$ thin film had a higher oxygen content. (With our notation we assume that oxygen reduction causes electron doping of the CuO_2 planes.) This film had a critical temperature of $T_c \approx 19$ K and resistivities of $\rho(30\ \mathrm{K}) \approx 55\ \mu\Omega\,\mathrm{cm}$ and $\rho(300\ \mathrm{K}) \approx 240\ \mu\Omega\,\mathrm{cm}$.

Overdoped sample (E96-368). The overdoping in this sample was accomplished by an increased Ce content whereas the oxygen content was optimal. This $Nd_{1.82}Ce_{0.18}CuO_{4\pm y}$ thin film had a critical temperature of $T_c \approx 20$ K and resistivities of $\rho(30\ \mathrm{K}) \approx 22\ \mu\Omega\,\mathrm{cm}$ and $\rho(300\ \mathrm{K}) \approx 220\ \mu\Omega\,\mathrm{cm}$.

The low resistivities, the sharp resistive transitions into the superconducting state (see Sec. V), and the high critical temperature of the optimally doped sample confirm the high quality of the thin films under investigation. The films were patterned into a Hall-bar geometry by standard photolithographic methods and Ar-ion-beam etching as shown in Fig. 1. The Hall bridges *A*, *B*, and the main bridge *C* were 100 μm and 500 μm wide, respectively, and about 5 mm long. Silver pads served as electrical contacts for current leads ($a-f$) and voltage probes (1–6). Isolated contact pads on the substrate were introduced as final heat sinks for the wiring.

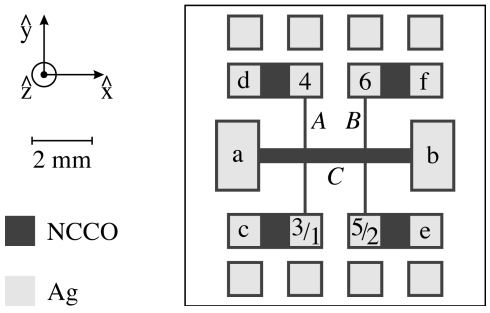

FIG. 1. Hall-bar geometry of the samples.

III. EXPERIMENTAL SETUP

The measurements were performed in an automated superconducting 11-T system where the magnetic field was oriented perpendicular to the thin films in the *z* direction ($\equiv c$ direction of the samples). The basic experimental setup already has been described in Ref. 10 and has been used for studies in the mixed state of $YBa_2Cu_3O_{7-\delta}$ and $Bi_2Sr_2CaCu_2O_{8+x}$. Here we used a new sample holder that allowed a continuous adjustment of the thermal coupling of the sample to the liquid-helium bath.[11] In this way a temperature range between 13 K and 300 K was accessible without interrupting the experimental session or exposing the sample to exchange gas. At lower temperatures we used a small amount of helium gas in the sample chamber since the establishment of a temperature gradient across the sample requires a stronger thermal coupling to the liquid-helium bath. In this temperature range the exchange gas was not critical for the measurements because the sample was shielded against the cold surrounding by copper sheets.

The electric transport coefficients have been determined using dc current sources and nanovoltmeters. After changes of temperature, external magnetic field *B*, or applied current *I* the system was allowed to stabilize before data points were taken. Currents were in the range $10-60\ \mu$A corresponding to current densities of 20–120 A/cm^2. The measurements have been performed for both directions of *I* and *B*. In magnetic-field sweeps at constant *T*, data points were taken for both sweep directions. The appropriate direction averages of the electric voltages across the main bridge and the Hall strips have been taken to isolate the longitudinal and transversal effects. An analysis of the magnetoresistivity $\Delta\rho/\rho(B)$ requires a careful determination of the temperature in the presence of the external magnetic field. We used Pt100 sensors from about 100 K to room temperature and carbon glass resistors at lower *T* to measure and control the temperature. The magnetic-field dependence of the temperature signals of these sensors caused corresponding temperature changes during magnetic-field sweeps. The experimental data were corrected afterwards for these temperature changes. The magnetic-field dependence of the platinum sen-

sors was known in the temperature range between 90 K and 150 K from previous measurements with a capacitance temperature sensor. We used tabulated values for the two sensor types to extend the magnetic-field-dependent corrections of the measured temperature to the whole T range of our investigations.[12,13] This turned out to be sufficiently accurate due to the large magnetoresistivity observed for NCCO. With our procedure, even at 300 K the relative error for $\Delta\rho/\rho(B)$ in this material was estimated to be no larger than 10%.

The thermoelectric effects also have been measured by a dc method. The sample was mounted between two gold-plated copper blocks that were seperated by about 5 mm. By adjusting a temperature difference between these copper blocks a temperature gradient could be applied in the x direction (as defined by Fig. 1). We used the Hall bars of the sample itself as resistive temperature sensors to determine $\nabla_x T$ with high accuracy. The temperature gradient across the sampe was typically 1–2 K/cm. Again, measurements have been performed for both directions of $\nabla_x T$ and the external magnetic field B as well as for both sweep directions. For an evaluation of the absolute thermopower of the NCCO samples the contribution of the copper leads to the measured Seebeck voltage $S_{\mathrm{TC}}=S_{\mathrm{NCCO}}-S_{\mathrm{Cu\ leads}}$ has to be known. We therefore determined the thermopower of the copper wiring relative to a lead film on $SrTiO_3$. The absolute thermopower of lead was tabulated by Roberts.[14] Above 70 K the absolute thermopower of the copper leads was in very good agreement with that of pure copper as reported in Ref. 15. At low temperatures the thermopower of the wiring was known with high accuracy from measurements against NCCO in the superconducting state. Further details of the experimental setup can be found in Ref. 11.

IV. NORMAL-STATE TRANSPORT PROPERTIES

A. Theoretical background

Several authors suggested a two-carrier picture to account for the observed temperature and doping dependences of the normal-state transport properties in the electron-doped cuprates.[6,16–18] The main aspects of the two-carrier picture can already be demonstrated in its most basic form, the Drude-type two-band model. Here, each band is characterized by a small set of transport coefficients. The simplicity of the model in principle allows one to isolate the transport properties of the single bands from measurements of a discrete set of transport coefficients. But there are some arguments against such a simple treatment of the transport properties of NCCO. In particular, the origin of the proposed two conduction bands remains unclear. Measurements of the Fermi surface (FS) by ARPES only resolved a single hole-like FS, although the resolution might not be sufficient to disclose parts with electronlike curvature.[5,19] These findings are consistent with band-structure calculations.[20] Consequently, we have to assume that there is only one FS of a single band present with possibly strongly varying local properties. Harris *et al.* derived expressions for the electrical transport coefficients of a two-dimensional (2D) metal with tetragonal symmetry within standard Boltzmann theory using a relaxation time approximation.[21] Their results can be regarded as justifications for the two-band model if the FS can be divided into two dominating zones corresponding to the two types of charge carriers. In the following we will briefly restate the main aspects of the Drude-type two-band model as well as the calculations in Ref. 21. Afterwards we will present an analysis of the thermomagnetic effects similar to that of the electric transport coefficients given by Harris and co-workers. We will describe the Seebeck coefficient S, the Nernst coefficient ν, and the magnetothermopower $\Delta S(B)$ as conductivity-weighted averages on the FS. These expressions can be translated back into a two-carrier picture leading to a more realistic two-band model that in principle might be suitable to isolate the thermopowers of the single zones (or bands) from measurements of the thermomagnetic effects. If the n-type systems, indeed, can be described within such a simple two-carrier picture, this might have implications for our general understanding of high-temperature superconductivity. A quantitative analysis of experimental data on NCCO will be given in the following subsection.

We consider a geometry with an external magnetic field $\boldsymbol{B}=B\mathbf{e}_z$ applied perpendicular to the xy plane of conduction in a two-dimensional metal with tetragonal symmetry ($\boldsymbol{e}_z=\boldsymbol{e}_x\times\boldsymbol{e}_y$ with $\boldsymbol{e}_i$ $(i=x,y,z)$ the unit vector in the i direction). The transport coefficients will be defined via the linear response of the system to small applied fields or currents:

$$\boldsymbol{E}=\hat{\boldsymbol{\rho}}\cdot\boldsymbol{j}+\hat{\boldsymbol{S}}\cdot\nabla T, \tag{4.1}$$

$$\boldsymbol{j}=\hat{\boldsymbol{\sigma}}\cdot\boldsymbol{E}-\hat{\boldsymbol{L}}\cdot\nabla T. \tag{4.2}$$

Here, $\hat{\boldsymbol{\rho}}$, $\hat{\boldsymbol{S}}$, $\hat{\boldsymbol{\sigma}}$, and $\hat{\boldsymbol{L}}$ are tensors of rank 2 for the resistivity, thermopower, conductivity, and thermoelectric conductivity, respectively. These are related by $\hat{\boldsymbol{\rho}}=\hat{\boldsymbol{\sigma}}^{-1}$ and $\hat{\mathbf{S}}=\hat{\boldsymbol{\rho}}\cdot\hat{\boldsymbol{L}}$. Because of the fourfold symmetry assumed in our system, for all such tensors $\hat{\boldsymbol{A}}$ we have $A_{xx}=A_{yy}$ and $A_{yx}=-A_{xy}$, where the first index k of A_{kl} corresponds to the direction of the ''driving force'' on the right-hand side of Eqs. (4.1) $(\boldsymbol{j},\nabla T)$ and (4.2) $(\boldsymbol{E},\nabla T)$, whereas l refers to the resulting component of the vectors on the left-hand side ($\boldsymbol{E}$ and $\boldsymbol{j}$, respectively). In the limit of small magnetic fields, the components A_{kl} can be expanded in powers of B. Whereas the symmetric parts of these tensors (describing the longitudinal effects) are even functions of the magnetic field, the antisymmetric parts (describing the transversal Hall effects) are odd functions of B. We consider contributions up to quadratic order in B in the symmetric and up to linear order in the antisymmetric part of all tensors. In particular we get $\rho_{xx}=\rho[1+\Delta\rho/\rho(B)]$, $\rho_{xy}=R_H B$, $S_{xx}=S+\Delta S(B)$, and $S_{xy}=\nu B$ with the resistivity in zero magnetic field ρ, the magnetoresistivity $\Delta\rho/\rho(B)\propto B^2$, the Hall coefficient R_H, the Seebeck coefficient in zero magnetic field S, the magnetothermopower $\Delta S(B)\propto B^2$, and the Nernst coefficient ν. In a similar way σ denotes the conductivity for $B=0$, etc.

Let us consider the case of two independent conduction bands. The transport coefficients of the combined system can be determined from those of the individual bands if we assume that the conductivities of the single bands add up to the total conductivities, leading to

$$\hat{\boldsymbol{\rho}}=(\hat{\boldsymbol{\sigma}}^{+}+\hat{\boldsymbol{\sigma}}^{-})^{-1}, \tag{4.3}$$

$$\hat{\boldsymbol{S}}=\hat{\boldsymbol{\rho}}\cdot(\hat{\boldsymbol{\sigma}}^{+}\cdot\hat{\boldsymbol{S}}^{+}+\hat{\boldsymbol{\sigma}}^{-}\cdot\hat{\boldsymbol{S}}^{-}), \tag{4.4}$$

where + and − refer to the two bands, respectively. As a starting point we want to adopt a Drude-type picture where each of the bands consists of charge carriers with identical properties, respectively. If a transport current is applied to an isolated band of this type, all carriers are assumed to move with the same drift velocity. Consequently, there is no magnetoresistivity for the single band because for all charge carriers the Hall electric field exactly cancels the Lorentz force due to the magnetic field. In case of an applied temperature gradient we could argue in a similar way. Here, the thermodiffusion of the charge carriers due to the temperature gradient is compensated by the drift current due to the Seebeck electric field. Since there is no net current and all currents are carried by identical particles, we might assume as a first approximation that there are no observable magnetic-field effects at all. Returning to our two-band model, this leads to $(\Delta\rho/\rho)^{+},(\Delta\rho/\rho)^{-},\nu^{+},\nu^{-},\Delta S^{+},\Delta S^{-}\approx 0$. Starting from Eqs. (4.3) and (4.4) and collecting the lowest-order terms in B we get the well-known expressions

$$\rho=(\sigma^{+}+\sigma^{-})^{-1}, \tag{4.5}$$

$$R_H=\frac{(\sigma^{+})^2R_H^{+}+(\sigma^{-})^2R_H^{-}}{(\sigma^{+}+\sigma^{-})^2}, \tag{4.6}$$

$$\frac{\Delta\rho}{\rho}=\frac{\sigma^{+}\sigma^{-}(\sigma^{+}R_H^{+}-\sigma^{-}R_H^{-})^2}{(\sigma^{+}+\sigma^{-})^2}B^2, \tag{4.7}$$

$$S=\frac{\sigma^{+}S^{+}+\sigma^{-}S^{-}}{\sigma^{+}+\sigma^{-}}, \tag{4.8}$$

$$\nu=-\frac{\sigma^{+}\sigma^{-}(S^{+}-S^{-})(\sigma^{+}R_H^{+}-\sigma^{-}R_H^{-})}{(\sigma^{+}+\sigma^{-})^2}, \tag{4.9}$$

$$\Delta S=\nu\frac{\sigma^{+}\sigma^{-}(R_H^{+}+R_H^{-})}{\sigma^{+}+\sigma^{-}}B^2. \tag{4.10}$$

If $R_H^{+},S^{+}>0$ and $R_H^{-},S^{-}<0$, the signs of R_H and S depend on the magnitude of the coefficients for the individual bands as well as on the weights of the single bands given by their conductivities. The Nernst coefficient ν turns out to be negative, therefore carrying the same sign as for a type-II superconductor in the mixed state (compare Sec. V). ν and the (positive) magnetoresistivity $\Delta\rho/\rho(B)$ in principle can reach large magnitudes, whereas $\Delta S(B)$ can be small even if the Nernst coefficient is large. Not only the large values of ν and $\Delta\rho/\rho(B)$ but also the doping and temperature-dependent sign changes of the Hall coefficient R_H and the thermopower S observed in NCCO can easily emerge from such a model with two conduction bands of oppositely charged quasiparticles.

For a two-dimensional system with fourfold symmetry, Harris *et al.* used standard Boltzmann theory and a relaxation-time approximation to express electric-transport coefficients in terms of local properties of the FS.[21] In principle, the Boltzmann equation allows the determination of the distribution function $f_{\boldsymbol{k}}=f(\boldsymbol{k})$ that is caused by an external electric field or temperature gradient in the presence of an additional magnetic field. With $g_{\boldsymbol{k}}\equiv f_{\boldsymbol{k}}-f_0(\epsilon_{\boldsymbol{k}})$ the deviation of $f_{\boldsymbol{k}}$ from the Fermi distribution $f_0(\epsilon_{\boldsymbol{k}})=[1+\exp\{(\epsilon_{\boldsymbol{k}}-\mu)/(k_BT)\}]^{-1}$, $\epsilon_{\boldsymbol{k}}$ the energy of an electron in the state $\boldsymbol{k}$, μ the chemical potential, e the electron charge, and $\boldsymbol{v}_{\boldsymbol{k}}=(1/\hbar)\nabla_{\boldsymbol{k}}\epsilon_{\boldsymbol{k}}$ the group velocity, the Boltzmann equation is given by[22]

$$\left.\frac{df_{\boldsymbol{k}}}{dt}\right|_{drift}=-\left.\frac{df_{\boldsymbol{k}}}{dt}\right|_{collision},$$

$$\left.\frac{df_{\boldsymbol{k}}}{dt}\right|_{drift}=-\frac{\partial f_0}{\partial\epsilon}(\epsilon_{\boldsymbol{k}})\boldsymbol{v}_{\boldsymbol{k}}\cdot\boldsymbol{F}_{\boldsymbol{k}}+\frac{|e|}{\hbar}(\boldsymbol{v}_{\boldsymbol{k}}\times\boldsymbol{B})\cdot\nabla_{\boldsymbol{k}}g_{\boldsymbol{k}}, \tag{4.11}$$

$$\boldsymbol{F}_{\boldsymbol{k}}=\left\{-|e|\boldsymbol{E}-\frac{\epsilon_{\boldsymbol{k}}-\mu}{T}\nabla T\right\}.$$

Again, we only consider small applied fields or temperature gradients. In general, a detailed knowledge of the scattering processes is required to formulate the collision term in Eq. (4.11). The solution of the Boltzmann equation is considerably simplified if a relaxation-time approximation is justified, i.e.,

$$\left.\frac{df_{\boldsymbol{k}}}{dt}\right|_{collision}=-\frac{g_{\boldsymbol{k}}}{\tau_{\boldsymbol{k}}}, \tag{4.12}$$

where the local relaxation time $\tau_{\boldsymbol{k}}$ is independent of the cause for the deviations from the equilibrium distribution ($\boldsymbol{E}$, ∇T, and $\boldsymbol{B}$) and therefore independent of $g_{\boldsymbol{k}}$. Then, $g_{\boldsymbol{k}}$ can be determined by an iterative procedure. We first consider the case $\boldsymbol{E}\neq 0$, $\nabla T=0$. To lowest order, $g_{\boldsymbol{k}}$ is due to the electric field, whereas the magnetic induction causes higher-order corrections:

$$g_{\boldsymbol{k}}^{(0)}=\left(-\frac{\partial f_0}{\partial\epsilon}(\epsilon_{\boldsymbol{k}})\right)\tau_{\boldsymbol{k}}\boldsymbol{v}_{\boldsymbol{k}}\cdot(-|e|\boldsymbol{E}),$$

$$g_{\boldsymbol{k}}^{(n)}=\frac{|e|}{\hbar}\tau_{\boldsymbol{k}}(\boldsymbol{v}_{\boldsymbol{k}}\times\boldsymbol{B})\cdot\nabla_{\boldsymbol{k}}g_{\boldsymbol{k}}^{(n-1)},\quad n=1,2,3,\ldots. \tag{4.13}$$

It is convenient to map the k space in terms of the energy ϵ and the arc length parametrization s of the corresponding constant energy curves $[\boldsymbol{k}=\boldsymbol{k}(\epsilon,s)]$. In our geometry the tangential vector of the constant energy curves is given by $\boldsymbol{e}_t=-(\boldsymbol{v}_{\boldsymbol{k}}\times\boldsymbol{B})/(v_{\boldsymbol{k}}B)$. Therefore, the magnetic-field induced changes of the distribution function can be expressed as $g_{\boldsymbol{k}}^{(n)}=-(|e|B/\hbar)l_{\boldsymbol{k}}\partial_s(g_{\boldsymbol{k}}^{(n-1)})$, where $l_{\boldsymbol{k}}=\tau_{\boldsymbol{k}}v_{\boldsymbol{k}}$ is the local mean free path. The electric transport coefficients can be determined from the current density $\boldsymbol{j}$ that is induced by $g_{\boldsymbol{k}}=\Sigma_i g_{\boldsymbol{k}}^{(i)}$: $\boldsymbol{j}=(-|e|/2\pi^2\hbar)\int_{BZ}g_{\boldsymbol{k}}(\boldsymbol{v}_{\boldsymbol{k}}/v_{\boldsymbol{k}})ds\,d\epsilon$ (BZ is the Brillouin zone). $g_{\boldsymbol{k}}^{(i)}$ causes a contribution $\boldsymbol{j}^{(i)}$ of the order B^i to the total current density $\boldsymbol{j}$. The main longitudinal contribution is due to the electric field and given by $\boldsymbol{j}^{(0)}$. Here, $\boldsymbol{j}^{(1)}\propto B$ is perpendicular to $\boldsymbol{j}^{(0)}$ and the lowest-order term in the Hall current, whereas $\boldsymbol{j}^{(2)}$ is to lowest order responsible for the magnetoconductivity. The integral for $\boldsymbol{j}$ in good approximation reduces to a line integral over the Fermi curve $\boldsymbol{k}(s)=\boldsymbol{k}(\mu\approx\epsilon_F,s)$.[23] If ϑ is the angle between the electric-field direction and the normal of the Fermi surface $\boldsymbol{e}_n$

$=\boldsymbol{v}_{\boldsymbol{k}}/v_{\boldsymbol{k}}$, the conductivity in zero magnetic field is given by $\sigma=j_x^{(0)}/E_x=\int_{FS}\tilde{\sigma}(s)ds$ with the local conductivity on the Fermi surface

$$\tilde{\sigma}(s)=\frac{e^2}{2\pi^2\hbar}l(s)\cos^2\vartheta(s). \tag{4.14}$$

Harris *et al.* defined a local conductivity weight $\tilde{\Sigma}=\tilde{\sigma}(s)/\sigma$ and a conductivity-weighted average over the Fermi surface $\langle F(s)\rangle_{\tilde{\Sigma}}=\int_{FS}\tilde{\Sigma}(s)F(s)ds$. Furthermore, they introduced the local Hall angle

$$\tilde{\theta}(s)=-\left(\frac{|e|B}{\hbar\cos\vartheta(s)}\right)\frac{d[l(s)\sin\vartheta(s)]}{ds} \tag{4.15}$$

to deduce the global Hall angle θ_H and the magnetoresistivity to lowest order in B:

$$\theta_H=\langle\tilde{\theta}(s)\rangle_{\tilde{\Sigma}}, \tag{4.16}$$

$$\frac{\Delta\rho}{\rho}=\langle\tilde{\theta}(s)^2\rangle_{\tilde{\Sigma}}-\langle\tilde{\theta}(s)\rangle_{\tilde{\Sigma}}^2. \tag{4.17}$$

This formally very nice result is only achieved by the introduction of the not very illustrative definition of the local Hall angle in Eq. (4.15).

In the following we want to motivate a different definition of the local properties that in a certain way will simplify the treatment and the interpretation of the transport integrals. Due to the assumed fourfold symmetry of the FS, integrals over constant energy curves in our case actually are independent of the electric-field direction. Therefore, before carrying out the integration over s, we calculate the direction average of the integrand: $\langle F(\vartheta)\rangle_\vartheta=(1/2\pi)\int_0^{2\pi}F(\vartheta)d\vartheta$. [This can also be seen from our transport integrals. There are only terms that are either proportional to $F_1(\vartheta)=\sin\vartheta\cos\vartheta$ or proportional to $F_2(\vartheta)=\cos^2\vartheta$. If we compare the contributions to the integrals at s and $s'=s+L_{FS}/4$ (L_{FS} being the length of the Fermi curve), we see that F_1 changes sign whereas $F_2(\vartheta(s'))=\cos^2(\vartheta(s)+\pi/2)=\sin^2\vartheta(s)$. All other factors in the integrals are identical at s and s'. Integrals containing F_1 vanish, whereas F_2 can be replaced by the factor 1/2.] In this way we are able to define local transport coefficients that only reflect properties of the Fermi surface and the corresponding electronic states. Again, the conductivity can be expressed as an integral $\sigma=\int_{FS}\sigma(s)ds$, where the new defined local conductivity is given by

$$\sigma(s)=\frac{e^2}{2\pi^2\hbar}\langle l\cos^2\vartheta\rangle_\vartheta=\frac{e^2}{2\pi^2\hbar}\frac{l(s)}{2}. \tag{4.18}$$

(In the following, local quantities will be indicated by their argument s where they have to be distinguished from total transport coefficients.) From $\sigma_{xy}=j_y^{(1)}/E_x$ and $\langle l\sin\vartheta\,\partial_s(l\cos\vartheta)\rangle_\vartheta=-(l/2)l(d\vartheta/ds)$ we find the local Hall conductivity $\sigma_{xy}(s)=-\sigma(s)\theta(s)$, where the local Hall angle $\theta(s)$ is now given by

$$\theta(s)=-\left(\frac{|e|B}{\hbar}\right)l(s)\alpha(s). \tag{4.19}$$

Here, $\alpha(s)=(d\vartheta/ds)(s)$ is the local curvature of the Fermi curve that is positive for an electronlike and negative for a holelike section of the Fermi surface. This definition of $\theta(s)$ can easily be interpreted geometrically. Corresponding to the new local conductivity in Eq. (4.18) we define the local conductivity weight $\Sigma(s)=\sigma(s)/\sigma$ and the conductivity-weighted average over the Fermi surface $\langle F(s)\rangle_\Sigma=\int_{FS}\Sigma(s)F(s)ds$. In terms of this conductivity weighted average we get

$$\theta_H\approx\frac{\rho_{xy}}{\rho}\approx-\frac{\sigma_{xy}}{\sigma}=\langle\theta(s)\rangle_\Sigma. \tag{4.20}$$

The difference between Eqs. (4.14), (4.15) and our definitions of the local conductivity equation (4.18) and the local Hall angle equation (4.19) result in a modified expression for the magnetoresistivity. Starting from $\Delta\sigma(B)=j_x^{(2)}/E_x$ we are lead to the following definition of the local magnetoconductivity:

$$\frac{\Delta\sigma}{\sigma}(s)=-\theta(s)^2-\left(\frac{|e|B}{\hbar}\right)^2\left(\frac{dl}{ds}\right)^2. \tag{4.21}$$

The magnetoresistivity is then given by

$$\begin{aligned}\frac{\Delta\rho}{\rho}&=-\frac{\Delta\sigma}{\sigma}-(\theta_H)^2 \\ &=\left(\frac{|e|B}{\hbar}\right)^2\left\langle\left(\frac{dl}{ds}\right)^2\right\rangle_\Sigma+[\langle\theta(s)^2\rangle_\Sigma-\langle\theta(s)\rangle_\Sigma^2].\end{aligned} \tag{4.22}$$

In this form it is more transparent how variations of the local mean free path and the local curvature of the Fermi curve [see Eq. (4.19)] contribute to the magnetoresistivity.

In the following we will extend our discussion to the case of an applied temperature gradient. For this purpose we have to perform the following substitution in Eq. (4.13): $-|e|\boldsymbol{E}\rightarrow[(\epsilon-\mu)/T](-\nabla T)$. From $L=j_x^{(0)}/(-\nabla_x T)$ we find with Boltzmann's constant k_B:[23]

$$\begin{aligned}L&\approx-A(T)\left(\frac{d}{d\epsilon}\sigma\right)_{\mu\approx E_F}, \\ A(T)&=\frac{\pi^2}{3}(k_BT)\left(\frac{k_B}{|e|}\right).\end{aligned} \tag{4.23}$$

Relations of identical form hold between L_{xy} and σ_{xy} as well as between ΔL and $\Delta\sigma$. For the energy derivative of the conductivity we get

$$\left(\frac{d}{d\epsilon}\sigma\right)_{E_F}=\int_{FS}\sigma(s)\left(\frac{d\ln l(s)}{d\epsilon}+\frac{\alpha(s)}{\hbar v(s)}\right)ds, \tag{4.24}$$

where the first term inside the parentheses comes from the energy dependence of the local conductivity, whereas the second term accounts for the energy dependence of the size of the Fermi surface (note that the local conductivity is normalized to unit length of the Fermi curve). The Seebeck coefficient in zero magnetic field now reads

$$S=\rho L=\langle S(s)\rangle_\Sigma \tag{4.25}$$

with the local thermopower

$$S(s)=-A(T)\left(\frac{d\ln l(s)}{d\epsilon}+\frac{\alpha(s)}{\hbar v(s)}\right). \tag{4.26}$$

From the energy derivative of σ_{xy} we find

$$L_{xy}=-\sigma\langle\theta(s)[S(s)+U(s)]\rangle_\Sigma, \tag{4.27}$$

where $U(s)$ results from the energy dependence of the local Hall angle:

$$U(s)=-A(T)\left(\frac{d\ln l(s)}{d\epsilon}+\frac{d\ln\alpha(s)}{d\epsilon}\right) \tag{4.28}$$

$$=-A(T)\left[\frac{d\ln l}{d\epsilon}-\frac{\alpha}{\hbar v}-\frac{1}{\alpha}\frac{d^2}{ds^2}\left(\frac{1}{\hbar v}\right)\right].$$

Thus, the normalized Nernst voltage $E_y/\nabla_x T$ is given by

$$S_{xy}=\rho_{xy}L+\rho L_{xy} \tag{4.29}$$

$$=\langle\theta(s)\rangle_\Sigma\langle S(s)\rangle_\Sigma-\langle\theta(s)[S(s)+U(s)]\rangle_\Sigma.$$

This is in disagreement with the result of Clayhold [Eq. (8) of Ref. 24: $S_{xy}=\langle\theta\rangle_\Sigma\langle S\rangle_\Sigma-\langle\theta S\rangle_\Sigma$], which can be simply understood as the generalization of Eq. (4.9). In contrast, Eq. (4.29) emphasizes that even in the isotropic case there is a nonvanishing Nernst effect. In the isotropic case the local quantities are independent of s, and we get $\nu=-\theta_H U/B=-\sigma R_H U$. [Assuming that U is dominated by $(\partial\ln\tau/\partial\epsilon)$ and taking the 3D-expressions $\sigma=ne^2\tau/m^*$ and $R_H=1/ne$, we recover the familiar result $\nu=-(\pi^2k_B^2T/3m^*)(\partial\tau/\partial\epsilon)$.] Within our model we can also determine the magnetothermopower. From $\Delta L=-A(T)(d\Delta\sigma/d\epsilon)_{E_F}$ we find

$$\frac{\Delta L}{\sigma}=\left\langle S(s)\frac{\Delta\sigma}{\sigma}(s)\right\rangle_\Sigma-\langle 2U(s)\theta(s)^2\rangle_\Sigma-A(T)$$

$$\times\left(\frac{|e|B}{\hbar}\right)^2\left\langle 2\frac{d\ln l}{d\epsilon}\left[\left(\frac{dl}{ds}\right)^2+l\left(\frac{d^2l}{ds^2}\right)\right]\right\rangle_\Sigma. \tag{4.30}$$

The magnetothermopower then can be calculated from

$$\Delta S=\frac{\Delta\rho}{\rho}S+\frac{\Delta L}{\sigma}-\theta_H\frac{L_{xy}}{\sigma}. \tag{4.31}$$

In contrast to the magnetoresistivity, ΔS also does not vanish in the isotropic case, where we find $\Delta S(B)=-\theta_H^2U=-(\sigma^2R_H^2U)B^2$.

Equations (4.5) to (4.10) suggest that the two groups of charge carriers can be roughly characterized by six parameters $\rho^i=1/\sigma^i$, R_H^i, and S^i $(i=+,-)$. From measurements of the six quantities ρ, $\Delta\rho/\rho$, R_H, S, ΔS, and ν we could in principle isolate the contribution of the single zones (or bands) to the total transport coefficients. Such a procedure might help to identify the physical origin of the two groups of charge carriers if the underlying model is justified. On the one hand, we can indeed regard Eqs. (4.20), (4.22), and (4.25) as justifications for Eqs. (4.6)–(4.8) On the other hand, Eqs. (4.9) and (4.10) do not take into account the real physical origin of the thermomagnetic effects. Starting from the isotropic case, Eqs. (4.29)–(4.31) suggest the following ansatz for the single zones $(i=+,-)$: $S_{xx}^i=S^i-(\theta_H^i)^2U^i$, $S_{xy}^i=-\theta_H^iU^i$, $\theta_H^i=\sigma^iR_H^iB$. This ansatz leads to additional terms in Eqs. (4.9) and (4.10). Now, each zone (or band) i is characterized by the four parameters ρ^i, R_H^i, S^i, and U^i. Therefore we have to make further assumptions to determine these parameters from the six measured quantities. In our model the Hall coefficient for a single zone only reflects geometric properties of the FS and should be independent of temperature. Similarly, we have $U^i=S^i+2A(T)(\alpha^i/\hbar v^i)=S^i-W^iT$, where the new defined W^i again should be independent of T. From measurements at different temperatures it should be possible to isolate the contributions of the single zones or bands. In a first step, $\rho^i(T)$ and R_H^i have to be determined from the experimental data $\rho_{xx}(T,B)$ and $\rho_{xy}(T,B)$. In a second step, $S^i(T)$ and W^i follow from the electrical properties of the single zones and the experimentally observed thermomagnetic effects.

Finally, we want to make some remarks on the limitations of our treatment of the thermomagnetic effects. First of all, it is far from established that the relaxation-time approximation is justified for NCCO in the temperature range of interest. In general, we have to distinguish between an electric scattering time $\tau_{\mathbf{k}}^{el}$ and a thermal relaxation time $\tau_{\mathbf{k}}^{th}$ because inelastic scattering plays a different role in restoring the equilibrium distribution in the case of an applied electrical field on the one hand and in the case of an applied temperature gradient on the other hand. If electrons are predominantly scattered by phonons, the relaxation-time approximation generally fails for temperatures below the Debye temperature Θ_D.[22] Furthermore, we have neglected any phonon drag effects: An applied temperature gradient also leads to changes of the phonon distribution function that might considerably affect the thermoelectric effects via electron-phonon interaction. We will return to these problems when discussing the experimental results.

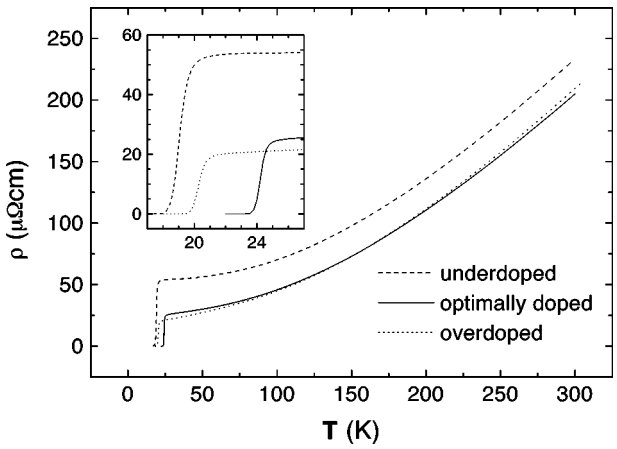

FIG. 2. Normal-state resistivities and superconducting transitions of the NCCO samples.

B. Experimental results

The normal-state resistivities and the resistive transitions into the superconducting state of the three NCCO thin films are shown in Fig. 2. For all samples ρ roughly exhibits a quadratic dependence on temperature. This has been inter-

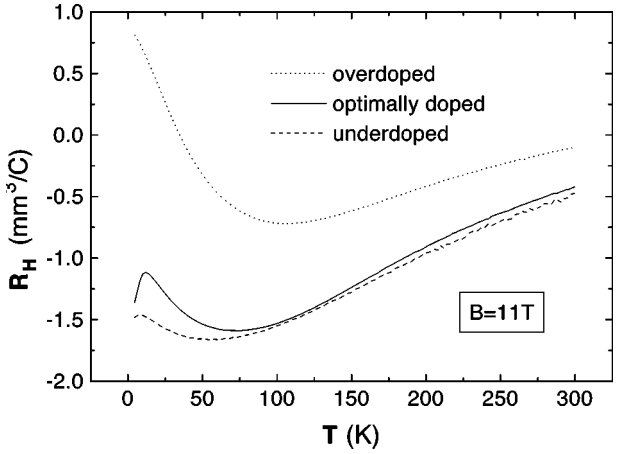

FIG. 3. Temperature dependence of the Hall coefficient.

preted as an indication for dominating electron-electron scattering in this material (see Ref. 25, and references therein). Indeed, at intermediate temperatures the resistivities can be well fitted to $\rho(T)=\rho_0+A_{ee}T^2$, whereas there is excellent agreement with the corresponding 2D formula $\rho(T)=\rho_0+K(T/T_F)^2\ln(T_F/T)$ for $T>150$ K. Here, Fermi temperatures $T_F=\epsilon_F/k_B$ between 5000 K and 6000 K were found for the different samples. At first sight, the resistivity of NCCO does not change very much with increasing doping. Basically, the differences could be simply interpreted as a reduction of impurity scattering from the underdoped to the overdoped sample. But we will see that there are real doping effects when we turn to the Hall effect and the magnetoresistivity.

The temperature dependences of the Hall coefficient R_H and the magnetoresistivity $\Delta\rho/\rho$ measured in a magnetic field of 11 T are shown in Fig. 3 and Fig. 4, respectively. At high temperatures all samples display a negative Hall constant. With decreasing temperature, R_H reaches a minimum and finally increases again towards positive values. Increasing electron doping results in a shift of R_H towards positive values, leading to a positive sign of the Hall constant for the overdoped sample at low temperatures. The temperature dependences of R_H and the cotangent of the Hall angle cot θ_H are complex for all samples and cannot be satisfactory described by power laws. A corresponding statement is true for the magnetoresistivity. At high temperatures $\Delta\rho/\rho$ is smallest for the underdoped and largest for the overdoped sample. With decreasing temperature there is a tendency for saturation of $\Delta\rho/\rho$ before superconducting fluctuations lead to a renewed increase. The normal-state magnetoresistivity of the NCCO thin films in good approximation obeys Kohler's rule although there are increasing deviations with increasing doping. In Fig. 5, a Kohler plot of $\Delta\rho/\rho$ is shown for the optimally doped sample. Clearly, there are considerable contributions to the magnetoresistivity from superconducting fluctuations at temperatures below 50 K. Therefore we have restricted the quantitative analysis of the electric transport properties within the two-band model to $T\geqslant 50$ K. The fact that Kohler's rule is not severely violated for our samples can be interpreted as a first encouraging test for the validity of our classical two-carrier picture.

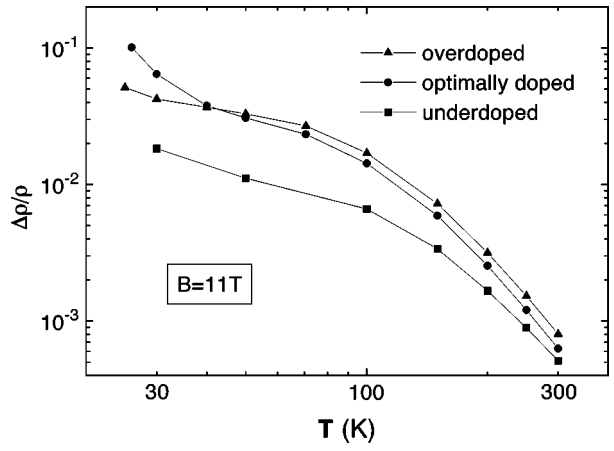

FIG. 4. Temperature dependence of the magnetoresistivity. The connecting straight lines are guides to the eye only.

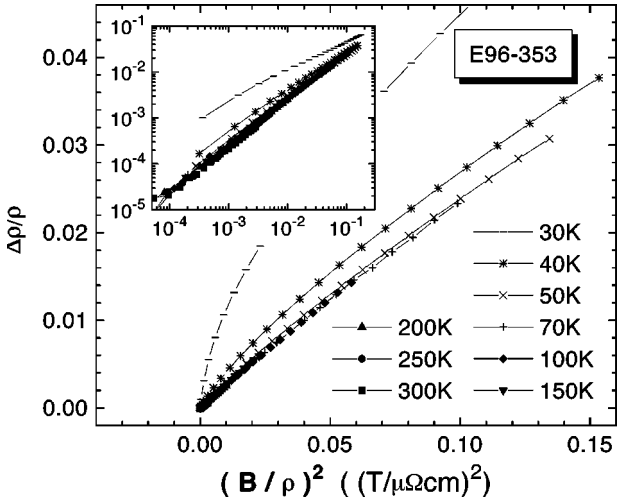

FIG. 5. Kohler plot of the magnetoresistivity data for the optimally doped sample. The inset displays the same data on a double-logarithmic scale.

As discussed in the previous subsection we assumed two bands (or zones of the Fermi surface) that can be characterized by temperature-independent Hall coefficients R_H^+ and R_H^-, respectively. As a result of our fitting procedure we get these two coefficients and the temperature-dependent resistivities of the two bands $\rho^+(T)$ and $\rho^-(T)$. We fitted experimental data from magnetic-field sweeps at different temperatures in the range 50 K$\leqslant T\leqslant$300 K. The two-band model is in very good agreement with the experimental data. This is demonstrated by Fig. 6 for the optimally doped sample. For the underdoped sample the fit was even better whereas it was somewhat worse for the overdoped NCCO thin film. This exactly reflects the degree to which the three samples obey Kohler's rule. Finally, the derived transport coefficients for the individual bands are summarized in Fig. 7. In addition to $\rho^i(T)$ and R_H^i $(i=+,-)$ we have plotted $\mu^i(T)=R_H^i/\rho^i(T)=\theta_H^i/B$ which is a measure for the mobility of the charge carriers in the isotropic case. As we can see from Eq. (4.19) in the more general case this quantity corresponds to the (local) product of the mean free path and the curvature of the FS: $\mu^i=(e/\hbar)l^i\alpha^i$. Before discussing the results in Fig. 7 we will first turn to the thermomagnetic effects in the normal state of our NCCO samples.

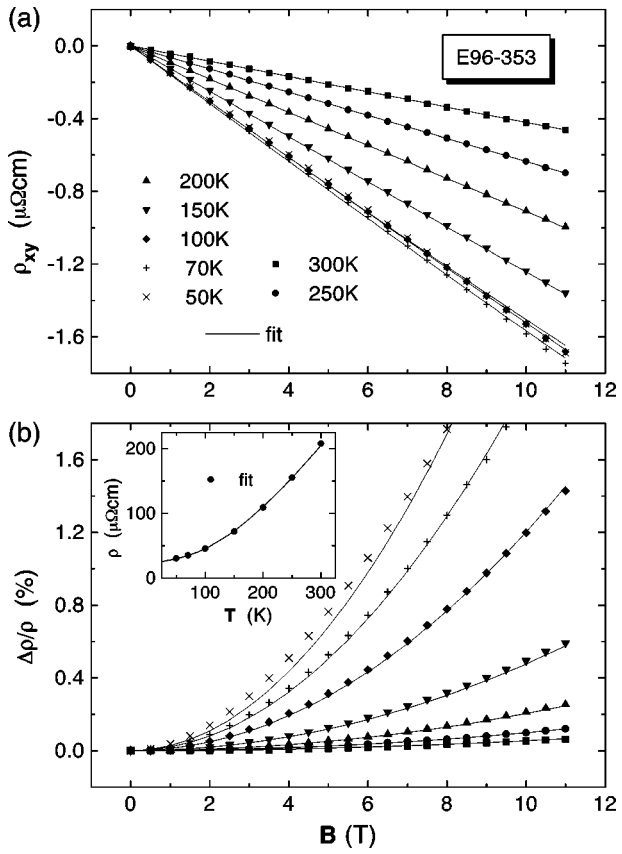

FIG. 6. Fit of the two-band model to experimental data for the optimally doped sample. The legend for the Hall data in (a) also applies to the magnetoresistivity data in (b). The inset in (b) displays the resistivity in zero magnetic field. Here, the solid line corresponds to the experimental data and the filled circles to the fitted values of the theory.

The temperature dependence of the Seebeck coefficient S is shown in Fig. 8. Similar to the behavior of the Hall constant, S shifts towards positive values with increasing electron doping. Whereas S is negative for the underdoped and the optimally doped sample there is a multiple sign change of the thermopower for the overdoped sample. The Nernst coefficient $\nu(T)$ as derived from the data for $B=11$ T is displayed in Fig. 9. Corresponding to our definition of ν, this coefficient is negative for all samples and temperatures. The magnitude of ν decreases with increasing electron doping. The relative drop of $|\nu|$ for the underdoped sample at low temperatures seems to be related to its larger residual resistivity. All samples display a very large magnetothermopower of negative sign. In Fig. 10, $\Delta S(B)$ at different temperatures is plotted for the optimally doped sample. Below 100 K there are clear saturation tendencies at large magnetic fields, i.e., beside the B^2 term higher-order contributions to $\Delta S(B)$ become important. Correspondingly, $S_{xy}(B)$ displays slight deviations from the linear behavior in this temperature range. Nevertheless, we tried to evaluate our two-carrier model as it was described in the previous subsection, but we did not succeed to fit the model to the experimental data. Obviously, the origin for the large magnitude of $\Delta S(B)$ is not properly taken into account by our simple model. This does not necessarily mean that the general idea of two-band conduction in NCCO fails. As we have already pointed out in the theoretical discussion, our model depends on the validity of the relaxation-time approximation. Also, phonon drag effects seem to play an important role for the thermoelectric effects in NCCO as is suggested by the local minima of the $S(T)$ data in Fig. 8 at temperatures below 100 K. (Considerable phonon drag effects have been reported for the p-type cuprate $YBa_2Cu_3O_{7-\delta}$.[26]) The position of the (supposed) phonon-drag peaks coincides with the temperature range where the large magnetothermopower is observed. Possibly, a detailed analysis of the phonon-drag contribution to the thermopower of NCCO might even help to clarify the significance of electron-phonon interaction for superconductivity in NCCO. Finally we want to point out that according to a previous study the large magnetothermopower does not seem to be a spin-related effect since $\Delta S(B)$ is small if the external magnetic field is oriented parallel to the CuO_2 planes in the direction of the temperature gradient.[27]

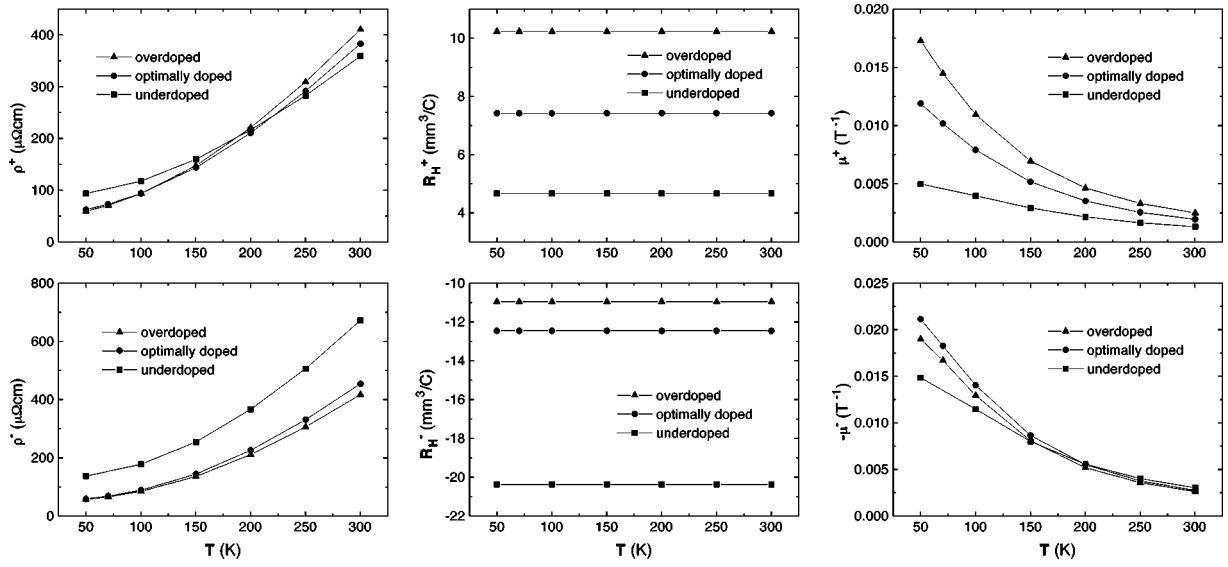

FIG. 7. Derived electrical transport coefficients of the single bands. The straight lines are guides to the eye. The temperature independence of R_H^+ and R_H^- has been presumed.

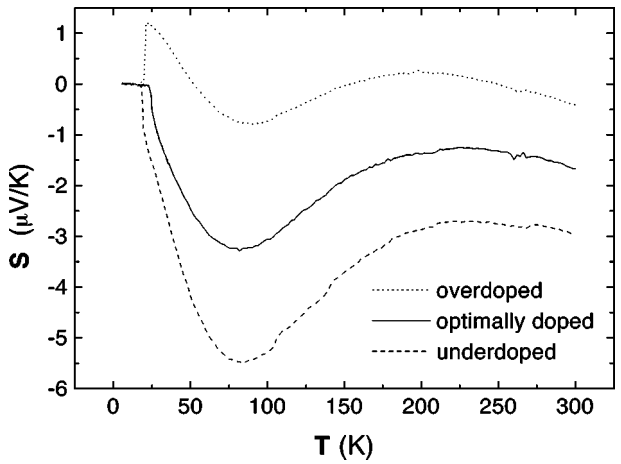

FIG. 8. Temperature dependence of the Seebeck coefficient.

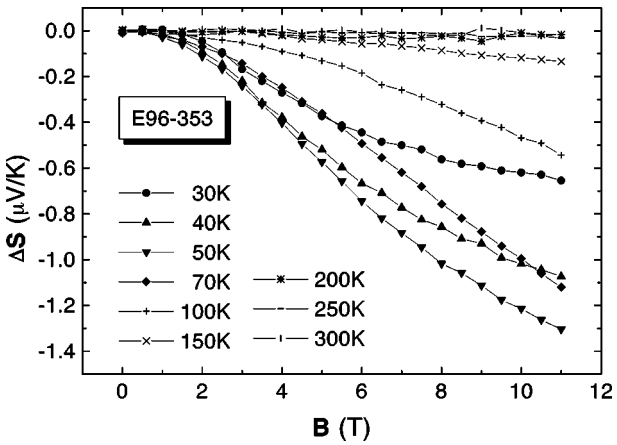

FIG. 10. Magnetothermopower at different temperatures for the optimally doped sample.

If we adhere to the idea of two-band conduction in NCCO, the doping dependence of the thermopower S and the large negative value of ν suggest that the two zones or bands have thermopowers $S^+>0$ and $S^-<0$, respectively, that almost cancel for the total system. In this case, $\Delta S(B)/S(0)$ can achieve large values and reflect subtle details of the band structure and the scattering mechanisms. In particular, $\Delta S(B)$ might be more sensitive to superconducting fluctuations than the magnetoresistivity. This possibly contributes to the failure to fit the experimental data on the thermomagnetic effects to the two-band model. We might still try to get a rough estimate for the thermopower of the single bands by introducing additional assumptions and fitting $S=S(B=0)$ and $S_{xy}(B)$ alone. For example, we might assume that for both bands the thermopower is dominated by the energy dependence of the mean free path. From Eqs. (4.26) and (4.28) we then find $U^i \approx S^i$ $(i=+,-)$. The result of the corresponding fitting procedure is shown in Fig. 11.

In principle, the ambitious aim of our discussion should be the disclosure of the origin of the electronlike and holelike contributions to the transport properties. Unfortunately, such a discussion would have a very speculative character at this time. After all, it is surprising that the electric transport coefficients of NCCO in the studied doping range can be described quantitatively within such a simple model. This gives confidence that the two-carrier (or two-zone) picture is in a certain way justified. In the following, we will therefore presume that the derived transport coefficients in Fig. 7 (and to a certain extent in Fig. 11) really describe two dominating groups of charge carriers.

As a first result we find that electronlike and holelike charge carriers are equally important for the transport properties of NCCO. This is in contrast to the analysis of Cruselas *et al.* on experimental data for a $Sm_{1.85}Ce_{0.15}CuO_4$ single crystal.[17] These authors concluded that the conductivity of the holelike band is dominating. The discrepancy is probably

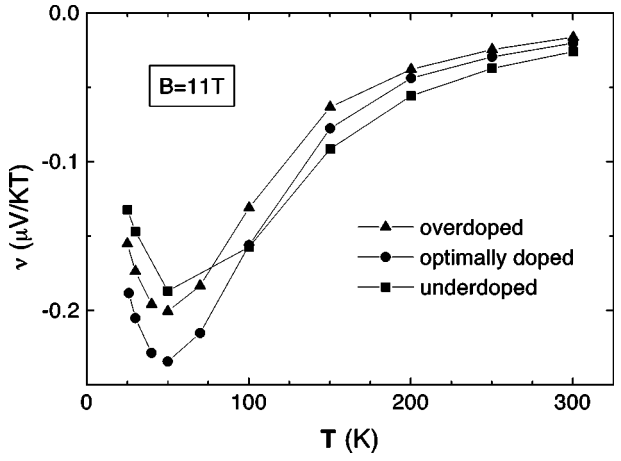

FIG. 9. Temperature dependence of the Nernst coefficient. The connecting straight lines are guides to the eye only.

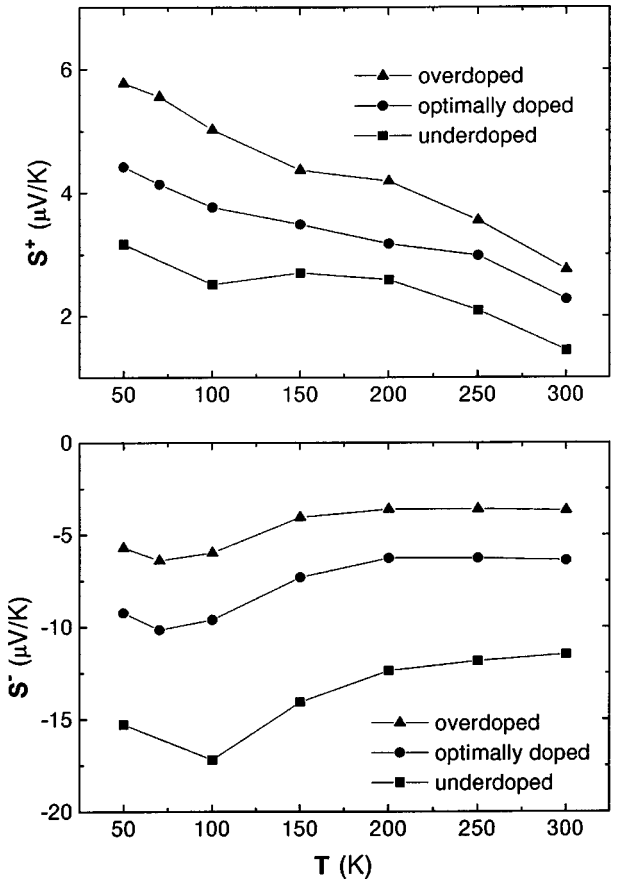

FIG. 11. Derived thermopowers of the single bands.

due to the fact that they only fitted the resistivity in zero magnetic field and the Hall effect while assuming certain temperature dependences for the resistivities of the single bands. Consequently, they observed only qualitative agreement of the magnetoresistivity data with their derived single-band parameters.

Secondly, our analysis did not reveal any severe differences between the doping effects by changing the oxygen content on the one hand and those by changing the Ce content on the other hand. Both ways of doping the NCCO thin films resulted in consistent variations of the transport properties of the isolated bands. Therefore our assumption that oxygen reduction is accompanied by electron doping of the CuO_2 planes seems to be justified. As a consequence, it should be possible, at least within certain limits, to compensate deviations of the Ce concentration from its optimal value by adjusting the oxygen content. This scenario opens a possible explanation for the extended superconducting concentration range that has been observed for $Pr_{2-x}Ce_xCuO_{4\pm y}$ single crystals by introducing a new reduction procedure,[28] though these findings still have to be confirmed by further studies.

In detail, the doping dependences for the single bands are as follows: For the electron band the mobility $\mu^- \propto l^- \alpha^-$ basically is independent of doping. This might be an indication that for the corresponding zone of the FS there are no drastic changes of the group velocity, the scattering time, and the curvature with increasing filling of the Brillouin zone. The changes of R_H^- and ρ^- could be ascribed to an increase of the size of the electronlike zone. In contrast, there is a considerable increase of the mobility with progressive doping for the holelike section of the FS whereas the resistivity does not change very much. The most simple way to explain this behavior is to assume an increase of the curvature of the holelike zone. Of course, the situation can be much more complicated. For example, we might think of a rapid increase of the group velocity when the FS is shifted away from a saddle point or of a decrease of the relaxation rate when the FS moves away from a region with strong scattering (as with the magnetic BZ boundary in the case of scattering by antiferromagnetic spin fluctuations).

We will close the discussion of the electric transport properties of the single bands by a comparision of $\rho^+(T)$ and $\rho^-(T)$. Roughly, both quantities share a quadratic dependence on temperature as it was observed for the total system. To emphasize the differences we have plotted the ratio $\rho^+/\rho^- = \sigma^-/\sigma^+$ in Fig. 12. By comparison with Fig. 3 we see how small changes of the ratio of the conductivities of the two groups of charge carriers result in the observed complex temperature dependence of the Hall coefficient R_H. A more careful analysis reveals that $\rho^-(T)$ can be very well approximated by the simple expression $\rho^-(T) = a + bT^2$ in the entire temperature range and for all samples. Similar to the total system, $\rho^+(T)$ exhibits deviations from this form and is better described by the corresponding 2D formula for dominant electron-electron scattering $\rho^+(T) = \rho_0^+ + K(T/T_F)^2 \ln(T_F/T)$ for $T > 150$ K. We do not think that these findings should really be interpreted in terms of differences in the dimensionality of the two bands. Possibly, these details depend on our simple model or on small errors in the determination of the magnetoresistivity.

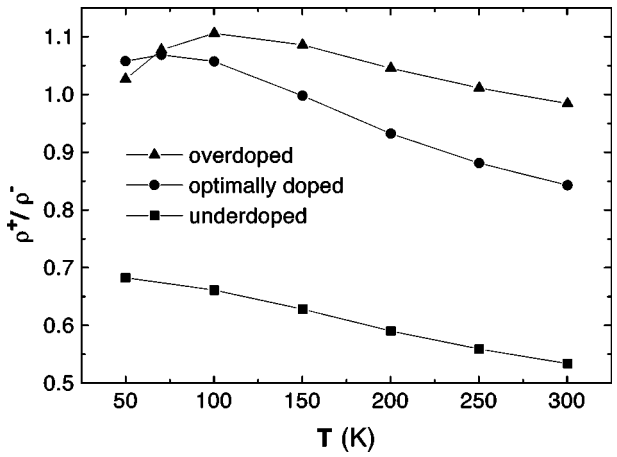

FIG. 12. Ratio of the resistivity of the holelike band to the resistivity of the electronlike band.

Finally, we will add some remarks on the thermopowers of the isolated bands, as shown in Fig. 11, although the plotted data can only be regarded as a first estimate for these quantities. Whereas S^+ and S^- shift towards positive values with progressive electron doping, they exhibit different temperature dependences. For S^+ roughly a linear T dependence can be observed, where the magnitude increases with decreasing temperature. The similarities to the thermopower of p-type HTSC's are noticeable. In contrast to S^+, the thermopower S^- displays a relative minimum that we have interpreted as a phonon-drag effect. A more detailed analysis of the thermomagnetic effects has to be performed in order to clarify if the influence of the phonon system is indeed different for holelike and electronlike charge carriers. This remains an interesting and challenging task for future studies.

V. SUPERCONDUCTING-STATE TRANSPORT PROPERTIES

A. Theoretical background

In the mixed state, p-type HTSC's exhibit transport properties that differ in many respects from those of the classical BCS superconductors. On the one hand, the layered structure, the high critical temperatures, and the small coherence lengths in the nm range cause a very rich phenomenology of vortex dynamics. Here, superconducting fluctuations play an important role. Depending on the degree of anisotropy and pinning, different (phase) transitions of the vortex lattice have been reported. The most prominent example probably is the broadening of the resistive transition in external magnetic fields. On the other hand, there is strong evidence for a d-wave pairing symmetry in the p-type cuprates. A discussion of the mixed state of a d-wave superconductor is still at the beginning. The vortex structure should also be affected if the superconductor is in the clean or even superclean limit as it is discussed for certain hole-doped HTSC's. Consequently, we have to introduce considerable modifications of concepts that have been established for classical BCS superconductors in the dirty limit.

In the case of the electron-doped HTSC's such as NCCO we probably deal with an s-wave superconductor. Therefore we possibly do not have to cope with the complications of

d-wave pairing. But still the strong anisotropy distinguishes this material from classical three-dimensional BCS superconductors. Also, NCCO is not in the dirty limit. In this paper we will concentrate on certain aspects of the superconducting-state transport properties of NCCO. Here, we will give a very brief overview of theoretical concepts that we used in our studies.

A major point will be the determination of the upper critical field from different measured quantities. Typical values reported for $B_{c2}(0)$ are not significantly higher than 8 T for NCCO. Therefore, this material can be driven into the normal state with accessible magnetic fields even at low temperatures. The most simple way to determine B_{c2} is from the shift of the resistive transition in an external magnetic field. This method gives reasonable values for classical BCS superconductors but does not work for *p*-type HTSC's due to the broadening of the resistive transition. In contrast, for NCCO there is no broadening but a real shift of the resistive transition in an applied magnetic field. Although superconducting fluctuations lead to a rounding of the transition, it is still possible to deduce a critical field from the position of the transition, e.g., by extrapolating its steep part to the normal-state value. Another possibility to determine the upper critical field is a fluctuation analysis of the resistivity. Since fluctuation theories usually are formulated in the framework of the time-dependent Ginzburg-Landau (GL) theory, this method is restricted to temperatures not too far from $T_c(H=0)$. Not too close to T_c, fluctuations are small and it is sufficient to treat the linearized GL equation leading to the theory of the so-called Gaussian fluctuations. In the case of NCCO a corresponding fluctuation analysis of the magnetoresistivity above T_c is complicated by the large normal-state contribution to $\Delta\rho/\rho$. Close to T_c, the nonlinear term in the GL equation has to be taken into account leading to the so-called critical fluctuations. In this critical region around T_c the fluctuation conductivity σ_{fluc} cannot be expressed in a closed form. Instead, scaling relations have been derived for σ_{fluc}.[29–31] Such scaling forms only exist in the limit of two and three dimensions, not for layered systems with arbitrary coupling of the superconducting planes. Ullah and Dorsey derived the following scaling relations for the fluctuation conductivity:

$$\sigma_{fluc}^{2D}=\left(\frac{T}{H}\right)^{1/2}\mathcal{F}_{2D}\left(\frac{T-T_{c2}(H)}{(TH)^{1/2}}\right), \tag{5.1}$$

$$\sigma_{fluc}^{3D}=\left(\frac{T^2}{H}\right)^{1/3}\mathcal{F}_{3D}\left(\frac{T-T_{c2}(H)}{(TH)^{2/3}}\right). \tag{5.2}$$

Here, we have already included all material specific parameters in the scaling functions $\mathcal{F}_{2D}$ and $\mathcal{F}_{3D}$. Close to T_c we have $T_{c2}(H)\approx T_c+H/(dH_{c2}^{ab}/dT)_{T_c}$. Thus, the scaling forms (5.1) and (5.2) depend on the two parameters T_c and $(dH_{c2}^{ab}/dT)_{T_c}$. These parameters can be determined for a given 2D or 3D sample by fitting the appropriate scaling relation to the experimental data.

The thermomagnetic effects in the mixed state are also suitable for a determination of the upper critical field. In contrast to the normal state, where these effects result from the diffusion of quasiparticles, there is another species that carries entropy and has a strong influence on the electrical transport properties: the magnetic flux lines. Whereas the thermodiffusion of quasiparticles is mainly responsible for the Seebeck effect in the mixed state, the diffusion of vortices predominantly results in a transversal voltage, i.e., in a Nernst effect.[10] In an applied temperature gradient a vortex experiences the thermal force per unit length

$$\boldsymbol{F}_{th}=-S_\phi\nabla T, \tag{5.3}$$

where S_ϕ is the transport entropy per unit length of the flux line. (In the following we will assume the same geometry as in the discussion of the normal-state properties: The temperature gradient is applied in the x direction and the external magnetic field is oriented perpendicular to our thin films in the z or c direction.) Without pinning, the thermal force is balanced by a viscous damping force: $\eta\boldsymbol{v}_\phi=\boldsymbol{F}_{th}$. The vortex moves opposite to the applied temperature gradient leading to an averaged electric field $\boldsymbol{E}=-\boldsymbol{v}_\phi\times\boldsymbol{B}$ in the negative y direction. The vortex entropy can be determined from measurements of the normalized Nernst electric field $S_{xy}=E_y/\nabla_x T$ if the damping coefficient η is known. This coefficient can be inferred from the flux-flow resistivity $\rho_{ff}=\phi_0 B/\eta$, where $\phi_0=h/2e$ is the flux quantum. We get

$$S_\phi=-\frac{\phi_0 S_{xy}}{\rho_{ff}}. \tag{5.4}$$

Pinning does not change this relation as long as it can be taken into account by a normalized damping coefficient.[32] The transport entropy can be connected to the reversible magnetization. Maki and Hu found in the framework of time-dependent GL theory[33,34]

$$S_\phi(T)=-\frac{\phi_0 M(T)}{T}L(T). \tag{5.5}$$

Here, $L(T)$ is a numerical factor that takes the value 1 close to T_c and 0 at $T=0$.[35] For low temperatures $L(T)$ is difficult to calculate and depends on material specific parameters. Within GL theory, Abrikosov found in the high-field limit $(H_{c2}-H\ll H_{c2})$

$$-M(T)=\frac{H_{c2}(T)-H}{\beta_A(2\kappa^2-1)+1}, \tag{5.6}$$

where κ is the Ginzburg-Landau parameter and $\beta_A\approx 1{,}16$ for a hexagonal vortex lattice. Close to T_c, the vortex transport energy per unit length of flux line $U_\phi=TS_\phi$ is given by

$$U_\phi(T)=\phi_0\frac{H_{c2}(T)-H}{\beta_A(2\kappa^2-1)+1} \tag{5.7}$$

with $H_{c2}(T)\approx(T-T_c)(dH_{c2}/dT)_{T_c}$. Close to the critical temperature, U_ϕ as well as $S_\phi\approx U_\phi/T_c$ therefore depend linearly on temperature and external magnetic field $B=\mu_0 H$. For fixed B, linear extrapolation of $U_\phi(T)$ or $S_\phi(T)$ to zero gives $T_{c2}(B)$. In addition to the upper critical field, the Ginzburg-Landau parameter κ can be derived from experimental data on $U_\phi(T)$ or $S_\phi(T)$. For extreme type-II superconductors $(\kappa\gg 1)$ we get

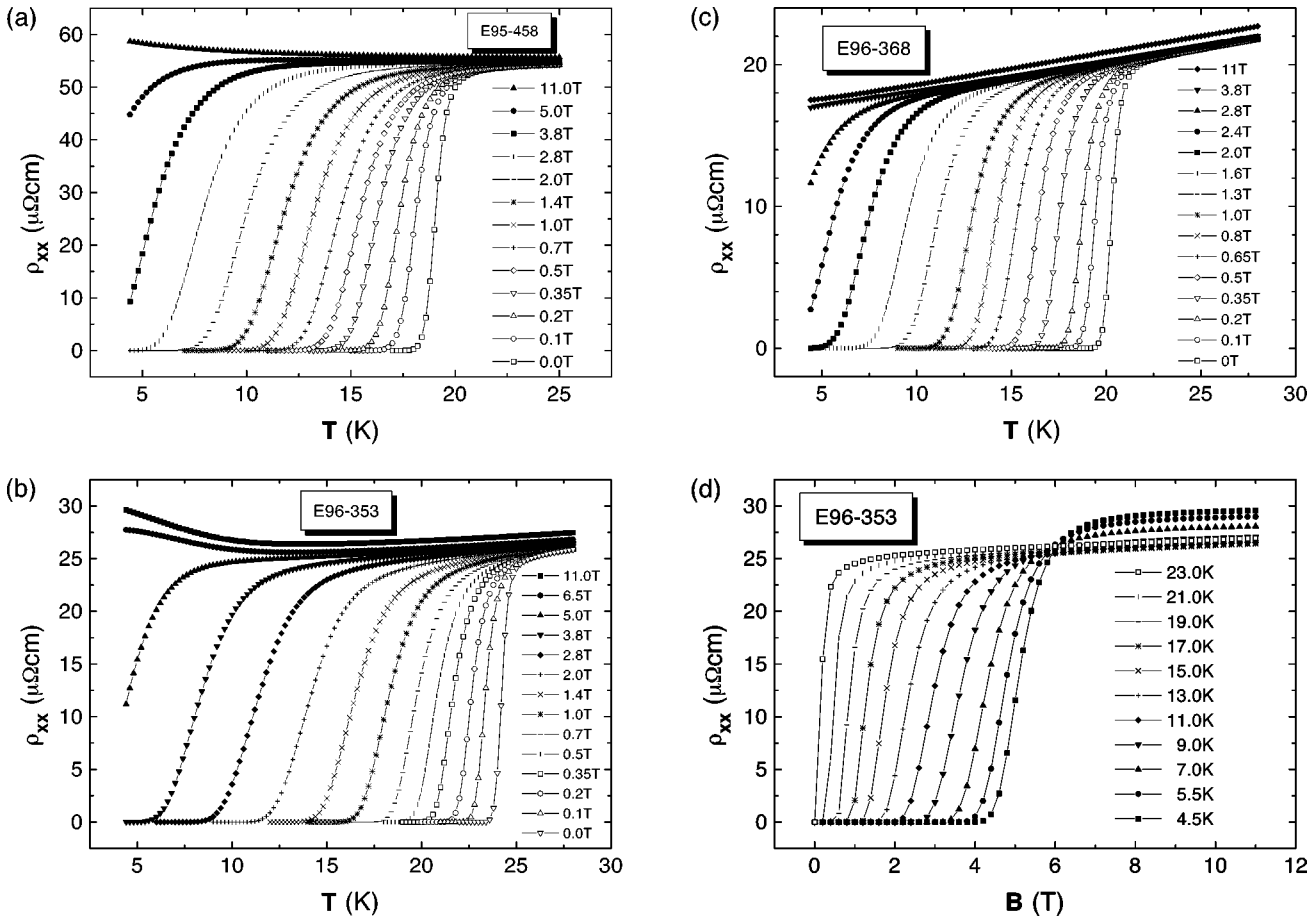

FIG. 13. Resistive transitions of the NCCO thin films in external magnetic fields. (a) $\rho(T)$ for the underdoped sample, (b) $\rho(T)$ for the optimally doped sample, (c) $\rho(T)$ for the overdoped sample, (d) $\rho(B)$ for the optimally doped sample.

$$\kappa \approx \sqrt{\frac{\phi_0}{2.32}\left(\frac{dH_{c2}/dT}{dU_\phi/dT}\right)_{T_c}}, \tag{5.8}$$

where (dU_ϕ/dT) is evaluated for small magnetic fields and temperatures close to T_c. In principle, the discussion of the transport energy can be extended to the intermediate field regime, e.g., by using the Hao-Clem result for the magnetization.[36,37] This has not been necessary in the case of NCCO. For high-κ materials deviations from the linear GL result can only be observed for B considerably smaller than the upper critical field.

B. Experimental results

A first characterization of the NCCO samples in the mixed state can be carried out on the basis of the resistive transitions in external magnetic fields. In Figs. 13(a)–13(c) we have plotted $\rho(T)$ curves for different applied fields, where the order of the graphs corresponds to increasing doping. Figure 13(d) gives exemplary $\rho(B)$ transitions for the optimally doped sample. The data indicate an increase of metallic properties with progressive doping in that sense that the normal-state resistivity ρ_n (measured in high magnetic fields) as well as its saturation tendency at low temperatures decreases. Remarkably, an almost linear T dependence of ρ_n is observed for the overdoped sample in the low-temperature range down to 4.2 K. In contrast, for the underdoped and the optimally doped sample ρ_n increases again for small T. Corresponding effects can also be observed for other transport coefficients (compare Fig. 3 for R_H or Fig. 20 for S). This sometimes has been attributed to localization effects. For all samples an increase of the external magnetic field results in a shift of the resistive transition to lower temperatures without appreciable broadening. For given temperature we have defined a resistive critical field B_ρ^* as the value of the applied field where $\rho(B)$ has reached half of its normal-state value. Correspondingly, B_ρ^* data can be deduced from $\rho(T)$ curves for fixed magnetic fields. In Fig. 14 we have plotted $B_\rho^*(T)$ for all samples as derived for all measured $\rho(T)$ and $\rho(B)$ transitions. We observe a positive curvature of $B_\rho^*(T)$ that decreases with increasing doping. This finding is independent of our 50% criterion for the definition of B_ρ^*. In Fig. 14 we have indicated the width of the resistive transition for the optimally doped sample as error bars. Here, the transition width has been determined by extrapolating the sharp rise of ρ to its normal-state value on the one side and to the value 0 on the other side. This is approximately equivalent to a 10–90 % criterion. Measurements of the resistive critical field of electron-doped cuprates have been reported for temperatures below 4.2 K with similar results.[38,39]

The observation of a positive curvature is not restricted to *n*-type HTSC's. Mackenzie *et al.* studied overdoped $Tl_2Ba_2CuO_6$ single crystals in magnetic fields up to 18 T and temperatures as low as 12 mK.[40] The samples exhibited T_c

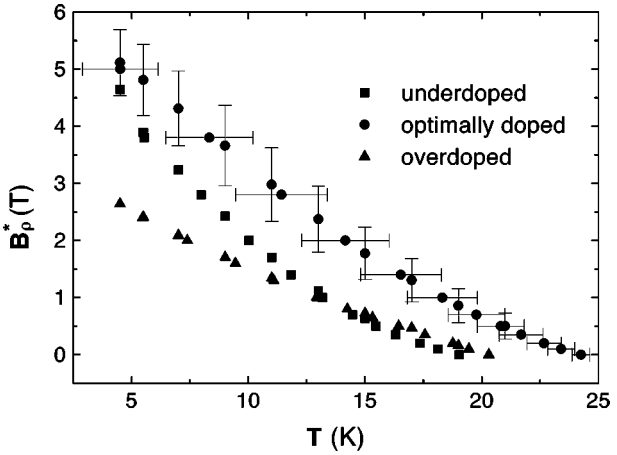

FIG. 14. Resistive critical fields for NCCO samples. The error bars for the optimally doped sample correspond to the transition widths.

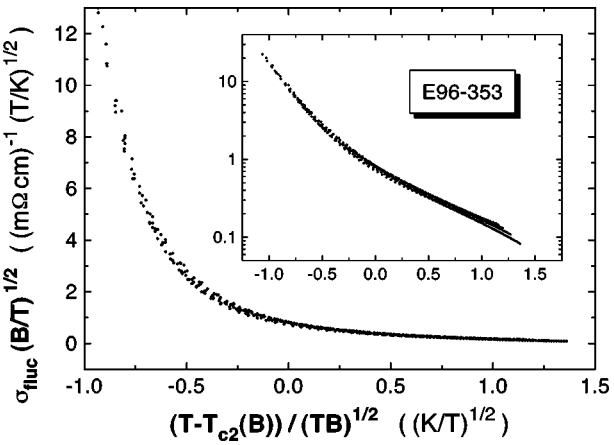

FIG. 15. 2D scaling of the fluctuation conductivity σ_{fluc} for the optimally doped sample with $T_c = 24.4$ K and $(dB_{c2}/dT)_{T_c} = -0.40$ T/K. The plot contains all experimental data with $15 < T \leq 28$ K, $1 \leq B \leq 5$ T, and $0.005\sigma_n \leq \sigma_{fluc} \leq 1.2\sigma_n$. The same data are shown in the inset on a logarithmic scale.

values of typically 20 K. Interestingly, the normal-state resistivities showed a quadratic dependence on temperature similar to that of our NCCO samples. Also, an applied magnetic field caused no broadening but a shift of the resistive transition. Down to the lowest temperatures, which corresponded to less than $0.001T_c$, the derived critical fields exhibited a positive curvature with no indications for a saturation, resulting in a rapid increase of B_ρ^* at low temperatures. At the same time, Osofsky *et al.* obtained similar results on $Bi_2Sr_2CuO_y$ thin films.[41] Later, Ovchinnikov and Kresin found very good agreement with this data when they included scattering on magnetic impurities into the calculation of the upper critical field B_{c2}.[42] However, there are still some doubts if the field B_ρ^* defined above can really be identified with B_{c2}. A study of the specific heat in $Tl_2Ba_2CuO_6$ resulted in higher critical fields than is suggested by the position of the resistive transition.[43] For the *n*-type cuprates the upper critical field was determined from the fluctuation conductivity σ_{fluc}.[44,45] Again, these values were larger than B_ρ^*. In Ref. 44 a 2D scaling behavior of σ_{fluc} was deduced for $Sm_{1.85}Ce_{0.15}CuO_4$ single crystals, whereas 3D scaling was reported for NCCO thin films in Ref. 45. We do not believe that there is a substantial difference in the dimensionality of these materials. Instead, we should emphasize that the determination of σ_{fluc} requires a good knowledge of the normal-state resistivity, especially for $T > T_c$ where fluctuation contributions to σ are relatively small. A certain shortcoming of the quoted two papers is that the pronounced normal-state magnetoresistivity has not been taken into account properly.

In the case of our NCCO thin films we have adopted the following procedure to determine σ_{fluc}. On the one hand, the normal-state magnetoresistivity $\Delta\rho_n/\rho_n$ of our samples is known with considerable accuracy since Kohler's rule is obeyed. $\Delta\rho_n/\rho_n$ is fitted as a function of $u \equiv (B/\rho_n)^2$ by a polynomial of low order. This is done for $T \geq 50$ K where superconducting fluctuations are small. On the other hand, we know from the Kohler plot, also, that magnetic-field-induced changes of ρ in the limit of very high B are basically given by the normal-state magnetoresistivity. In Fig. 5 we see for $T = 40$ K that $\Delta\rho/\rho$ at high fields is parallel to the magnetoresistivity at higher temperatures where fluctuation contributions can be neglected. For the optimally doped sample, this is reasonably fulfilled even for magnetoresistivity data at $T = 26$ K that are not shown in Fig. 5. Therefore, we can assume that superconducting fluctuation contributions to σ are effectively suppressed in magnetic fields of 11 T: $\sigma_{fluc}(T, B = 11\ \text{T}) \approx 0$, i.e., $\rho(T, B = 11\ \text{T}) \approx \rho_n(T, B = 11\ \text{T})$. With $\Delta\rho_n/\rho_n(u)$ and $\rho(T, B = 11\ \text{T})$ known, the fluctuation conductivity $\sigma_{fluc}(T,B)$ can be calculated from $\rho(T,B)$ via

$$\sigma_{fluc}(T,B) = \rho(T,B)^{-1} - \rho_n(T,B)^{-1}, \tag{5.9}$$

$$\rho_n(T,B) \approx \rho(T, 11\ \text{T}) \frac{1 + \Delta\rho_n/\rho_n(u(T,B))}{1 + \Delta\rho_n/\rho_n(u(T, 11\ \text{T}))},$$

$$u(T,B) = (B/\rho_n(T,0))^2 \approx (B/\rho(T, 11\ \text{T}))^2.$$

We restricted the scaling fit of σ_{fluc} according to Eqs. (5.1) and (5.2) to temperatures not too far from T_c and to intermediate magnetic fields. On the one hand, Eq. (5.9) does not give the correct fluctuation conductivity for $B \to 11$ T. On the other hand, the scaling forms of Eqs. (5.1) and (5.2) are valid only in the lowest Landau-level approximation, i.e., at high magnetic fields. In addition we restricted the fit to $0.005\sigma_n \leq \sigma_{fluc} \leq 1.2\sigma_n$ in order to limit the influence of pinning that starts to determine the resistive transition at large values of σ_{fluc}. For all samples the fluctuation conductivity was considerably better described by the 2D scaling form of Eq. (5.1). In Fig. 15 we have plotted the 2D scaled fluctuation conductivity for the optimally doped sample. 3D scaling did not result in such a good fit and the obtained values for $(dB_{c2}/dT)_{T_c}$ were unreasonably high. Only for the overdoped sample this quantity started to develop towards realistic values. This might be an indication that NCCO gradually changes from a 2D to a 3D system with increasing electron doping.

The 2D scaling of σ_{fluc} for the optimally doped sample was somewhat better than for the other samples. Due to different circumstances σ_{fluc} could not be determined as accu-

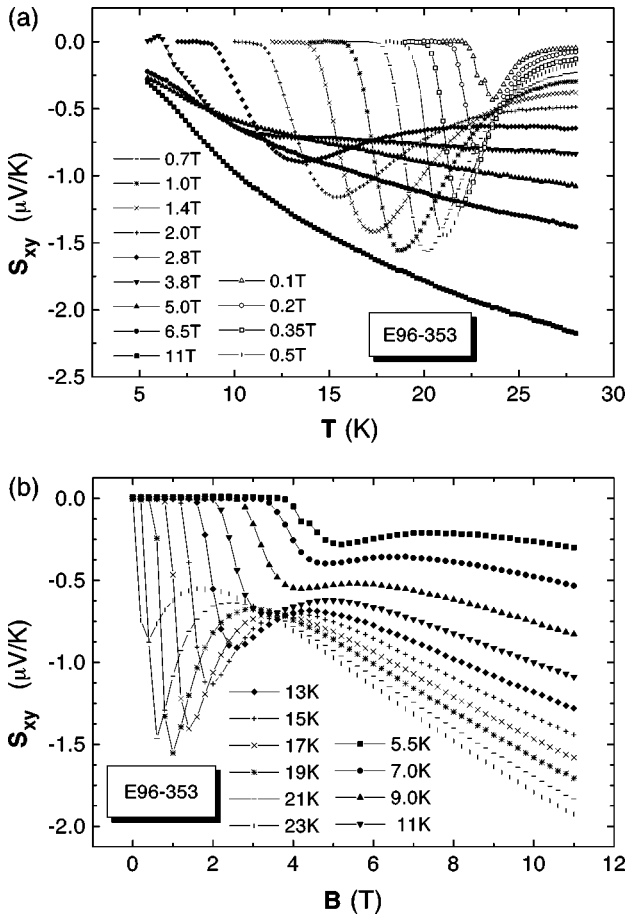

FIG. 16. Temperature (a) and magnetic-field dependence (b) of the normalized Nernst voltage $S_{xy}=E_y/\nabla_x T$ for the optimally doped sample.

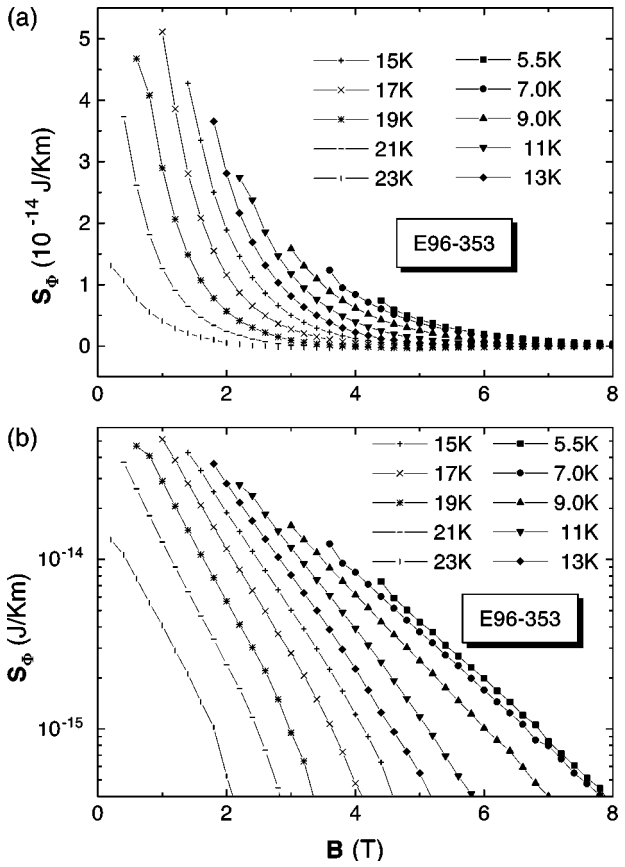

FIG. 17. Magnetic-field dependence of the vortex transport entropy for the optimally doped sample on a linear (a) and a logarithmic scale (b).

rately for the latter samples as for the optimally doped film. For the underdoped thin film, fluctuation effects were comparatively large so that the approximation $\sigma_{fluc}(T,B=11\ \mathrm{T})\approx 0$ did not work as well as for the other samples. This also can be interpreted as a signature of a pronounced 2D character of this material. In the case of the overdoped NCCO thin film, deviations of the magnetoresistivity from Kohler's rule did not allow an accurate extrapolation of $\Delta\rho_n/\rho_n$ to low temperatures. For the optimally doped sample we obtained $T_c\approx 24.4\pm 0.2$ K and $(dB_{c2}/dT)_{T_c}\approx -0.40\pm 0.01$ T/K. Here, we fitted experimental data with 15 K$<T\leqslant 28$ K and 1 T$\leqslant B\leqslant 5$ T. The errors were estimated by varying the temperature and magnetic-field range and the error weight in our fitting procedure. The small error values reflect that with the above parameters a reasonable scaling was observed even in the magnetic-field range between 0.2 T and 1 T as well as for temperatures down to 10 K. For the underdoped sample we obtained $T_c\approx 19.2\pm 0.2$ K and $(dB_{c2}/dT)_{T_c}\approx -0.63\pm 0.06$ T/K, whereas for the overdoped thin film $T_c\approx 20.5\pm 0.2$ K and $(dB_{c2}/dT)_{T_c}\approx -0.23\pm 0.03$ T/K were derived. Within the Werthamer-Helfand-Hohenburg (WHH)-theory[46] the upper critical field at $T=0$ can be calculated as $B_{c2}(0)\approx 0.69T_c|dB_{c2}/dT|_{T_c}$. The in-plane coherence length follows as $\xi_{ab}(0)=\sqrt{\phi_0/2\pi B_{c2}(0)}$. For the three samples we obtained (in the order of progressive electron doping) $B_{c2}(0)\approx 8.4$ T, 6.8 T, and 3.3 T and $\xi_{ab}(0)\approx 63$ Å, 70 Å, and 100 Å, respectively.

In the following we will turn to the determination of the upper critical field from the transport entropy (or energy) of magnetic flux lines. In Figs. 16(a) and 16(b) the temperature and magnetic-field dependence of the normalized Nernst voltage $S_{xy}=E_y/\nabla_x T$ is shown for the optimally doped sample. The large normal-state contribution can easily be identified on grounds of its linear dependence on B. As expected, the superconducting contribution due to the thermodiffusion of magnetic flux lines has the same (negative) sign. This contribution increases when the superconducting state is entered by reducing the temperature or external magnetic field. Its magnitude reaches a maximum before S_{xy} goes to zero due to pinning of the vortices. From general thermodynamic arguments we expect $S_{xy}\rightarrow 0$ for $T\rightarrow 0$ even without pinning. When calculating the vortex transport entropy $S_\phi=-\phi_0 S_{xy}/\rho$, pinning effects basically drop out. But we still have to correct this experimental quantity for normal-state contributions that are neglected in Eq. (5.4). Here we assume that the normal-state contribution at small fields can simply be determined by extrapolating $S_\phi(B)$ from higher fields. This appears reasonable since it is equivalent to the assumption that the normal-state contribution to S_{xy} is given by $(\rho/\rho_n)S^n_{xy}=(\sigma_n/\sigma)S^n_{xy}$, where S^n_{xy} is the normalized Nernst voltage in the normal state. Because to lowest order S^n_{xy} is

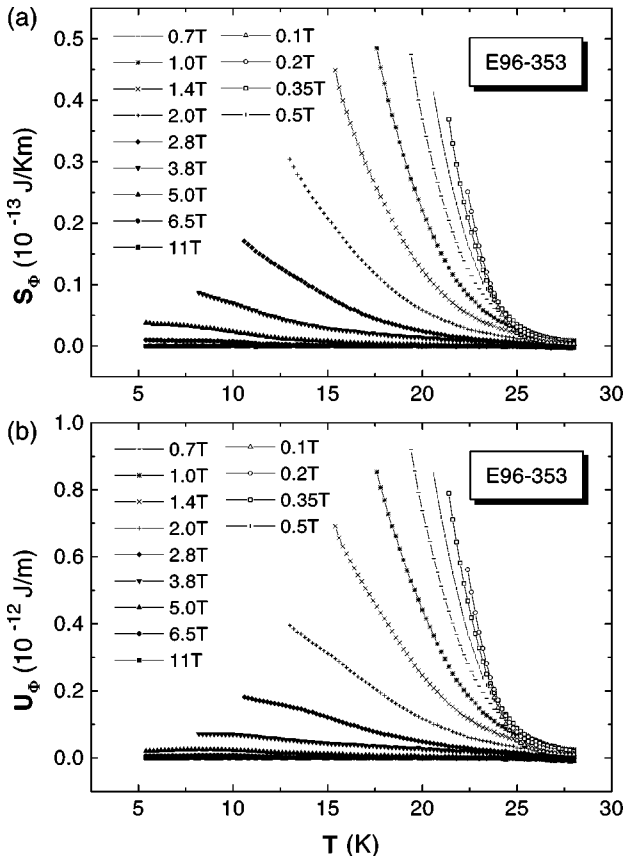

FIG. 18. Temperature dependences of the vortex transport entropy S_ϕ (a) and the vortex transport energy U_ϕ (b) for the optimally doped sample after correction of the normal-state contributions.

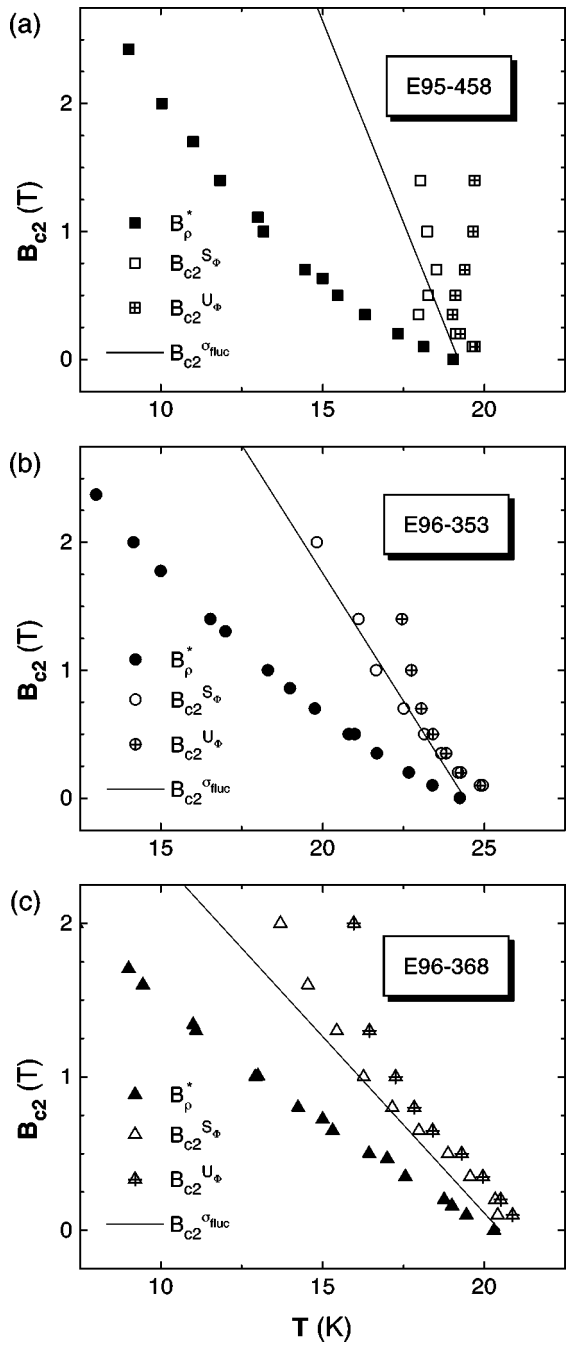

FIG. 19. Comparison of the temperature dependences of the upper critical fields derived from different transport properties. The upper critical field $B_{c2}^{fluc}(T)$ has been assumed linear in T corresponding to the approximation in the scaling analysis of $\sigma_{fluc}(T)$. The plots (a)–(c) are in the order of increasing electron doping.

proportional to B we performed a linear extrapolation of the high-field regime of $S_\phi(B)$ to approximate the normal-state background.

The corrected $S_\phi(B)$ data for the optimally doped sample are plotted in Fig. 17(a). It is very difficult to determine the upper critical field by linear extrapolation of $S_\phi(B)$ to zero. Instead of a linear dependence on B, as suggested by the GL theory, we observe an almost exponential decrease of $S_\phi(B)$ with increasing field. In Fig. 17(b) the vortex transport entropy is plotted on a logarithmic scale. We do not believe that the data already correspond to the low-field regime where deviations from linearity are expected.[36,37,47] Instead, fluctuation effects might play an important role even at low temperatures. Of course, the detailed magnetic-field dependence of our $S_\phi(B)$ data sensitively depends on the correction procedure for the normal-state contribution. Therefore, the exponential dependence of the vortex entropy on B might be an artifact, although this feature was observed for all samples. For the same reason we did not try a fluctuation analysis of the transport entropy.

For the optimally doped sample, the corrected quantities $S_\phi(T)$ and $U_\phi(T)$ for different applied fields are given in Figs. 18(a) and 18(b), respectively. Obviously, the T-dependent data are better suited for an analysis within the high-field GL formalism because $S_\phi(T)$ and $U_\phi(T)$ at least partly exhibit a linear dependence on temperature. For a given magnetic field we have determined the corresponding transition temperature by linear extrapolation of these two quantities to zero. There are two systematic sources for errors in the determination of the upper critical field. First of all, $S_\phi(T)$ and $U_\phi(T)$ are linear in T only close to the critical temperature for a given magnetic field. On the low-temperature side, both quantities finally have to go to zero as T approaches zero. Therefore $S_\phi(T)$ and $U_\phi(T)$ gradually flatten with decreasing temperature. On the high-temperature side, superconducting fluctuations also lead to a flattening of $S_\phi(T)$ and $U_\phi(T)$. Therefore, the linear extrapolation results in transition temperatures that are too high except for a certain intermediate magnetic-field range. This problem is more

TABLE I. Comparison of different material parameters. The order of the samples (top to bottom) corresponds to increasing electron doping.

Sample	T_c (K)	$-(dB_{c2}/dT)_{T_c}$ (T/K)	$B_{c2}(0)$ (T)	$\xi_{ab}(0)$ (Å)	$-(dU_\phi/dT)_{T_c}$ (J/K m)	κ	$\lambda(0)$ (Å)
E95-458	19.2	0.63	8.4	63	1.2×10^{-13}	61	3800
E96-353	24.4	0.40	6.8	70	3.2×10^{-13}	30	2100
E96-368	20.5	0.23	3.3	100	1.7×10^{-13}	31	3100

severe for the determination of the upper critical field from the transport energy because $U_\phi = TS_\phi$ contains an additional factor T. This can be seen by comparison of Figs. 18(a) and 18(b).

In Fig. 19 we have plotted the upper critical fields $B_{c2}^{S_\phi}$ and $B_{c2}^{U_\phi}$ that have been derived by linear extrapolation of $S_\phi(T)$ and $U_\phi(T)$, respectively. This procedure did not work well for the underdoped sample due to pronounced superconducting fluctuation contributions to these quantities. Because fluctuation effects decreased with progressive doping, the determination of the upper critical field by this method was most definite for the overdoped sample. This can also be seen in Fig. 19 by comparison with the upper critical field B_{c2}^{fluc} that has been derived from the scaling of the fluctuation conductivity. For temperatures not too far from T_c, there is good agreement between the differently derived B_{c2} data for the optimally doped and the overdoped sample. This gives some confidence that the fluctuation analysis results in an accurate value for the underdoped sample, also. In the following, we will therefore regard B_{c2}^{fluc} as the correct upper critical field of our samples. The resistive critical field B_ρ^* is also shown in Fig. 19. Obviously, B_ρ^* does not correspond to B_{c2} which is considerably larger for given temperature. This supports findings as given in Refs. 43–45. In particular, the theory of Ovchinnikov and Kresin does not seem to apply.[42] Possibly, the two-dimensional character of NCCO is responsible for the differences between B_ρ^* and B_{c2}. There are some arguments in favor of this assumption. The order of magnitude of superconducting fluctuations as well as our scaling analysis of σ_{fluc} indicate that the underdoped sample has a pronounced 2D character, which diminishes with increasing electron doping. With progressive doping we also observe a decrease of the positive curvature of $B_\rho^*(T)$ as well as a reduction of the discrepancy between B_ρ^* and B_{c2}. Finally, we compare the resistive critical field in Fig. 14 with the $B_{c2}(0)$ values that have been derived within our scaling analysis of σ_{fluc} and the WHH theory. For all samples, extrapolation to low temperatures indicates that B_ρ^* might take on the same value at $T=0$ as B_{c2}. Summing up it may be said that the positive curvature of the resistive critical field $B_\rho^*(T)$ does not necessarily conflict with the idea of classical superconductivity in NCCO. However, the quasi-2D character of this material and the resulting fluctuation effects have to be taken into account.

To complete our discussion of the Nernst effect in the mixed state we have determined the Ginzburg-Landau parameter κ according to Eq. (5.8). Because superconducting fluctuations and the numerical factor $L(T)$ in Eq. (5.5) reduce the slope $|dU_\phi/dT|$, we have determined its maximum value which was taken for small magnetic fields (0.2–0.5 T) and T close to T_c. The highest value $(dU_\phi/dT)\approx -3.2\times10^{-13}$ J/K m was found for the optimally doped sample that is comparable to that of $YBa_2Cu_3O_{7-\delta}$ (-2.5×10^{-13} J/K m).[10] For the underdoped sample we derived $(dU_\phi/dT)\approx -1.2\times10^{-13}$ J/K m and for the overdoped film $(dU_\phi/dT)\approx -1.7\times10^{-13}$ J/K m. The order of magnitude of (dU_ϕ/dT) is consistent with the predictions of the GL theory. Consequently, there are no indications for a reduction of the vortex transport entropy due to a quasiparticle bound-state quantization in the vortex core as suggested by Jiang *et al.*[48] These authors obviously used S_ϕ data from the fluctuation regime to perform their analysis. From (dU_ϕ/dT) and Eq. (5.8) we derived Ginzburg-Landau parameters $\kappa = 61$, 30, and 31 for the underdoped, the optimally doped, and the overdoped sample, respectively. The London penetration depth is minimal for the optimally doped sample. In the order of progressive doping we found $\lambda(0) = \kappa\xi_{ab}(0) = 3800$ Å, 2100 Å, and 3100 Å. $\lambda(0) = 2100$ Å is about 60% larger than values that have been determined from the surface resistance [in Ref. 3: $\lambda(0)\approx 1300$ Å for $Nd_{1.85}Ce_{0.15}CuO_{4\pm y}$ thin films on $LaAlO_3$]. The material parameters that have been derived for the three samples are summarized in Table I. A similar listing for the *p*-type HTSC's $YBa_2Cu_3O_{7-\delta}$ and $Bi_2Sr_2CaCu_2O_{8+x}$ can be found in Ref. 10.

We also performed measurements of the Seebeck effect in the mixed state. In the dirty limit $S\approx(\rho/\rho_n)S_n$ is expected, where S_n is the thermopower in the normal state. Deviations from this relation have been observed in the *p*-type HTSC's, which have been ascribed to a reduction of the quasiparticle scattering rate in the superconducting regime.[10,49–52] Unfortunately, the large magnetic-field dependence of the normal-state thermopower did not allow a detailed analysis of the Seebeck effect in the mixed state of NCCO. Exemplary experimental data for the optimally doped sample are given in Fig. 20. The sign changes of S for certain temperatures and magnetic fields obviously have nothing to do with the entry into the superconducting regime but are related to a sign change in the normal state. In high magnetic fields the slope of $S(T)$ changes its sign at about 12 K. This seems to be related to similar features in the resistivity and the Hall coefficient. The sharp double-peak structures that have been observed for this sample in the foot of the superconducting transition are artifacts that have technical reasons.[11]

We will close our discussion of the superconducting-state transport properties with some remarks on the Hall effect. The magnetic-field dependence of the Hall coefficient R_H for the optimally doped sample is plotted in Fig. 21. There are no indications for a sign change of R_H when entering the

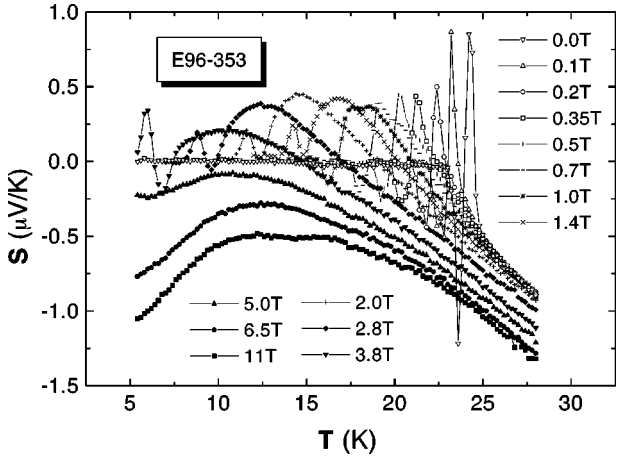

FIG. 20. Temperature dependences of the thermopower S for the optimally doped sample.

superconducting state. Also, the scaling behavior of the Hall effect in NCCO is different from that of p-type HTSC's. In $YBa_2Cu_3O_{7-\delta}$ $\rho_{xy}(T,B) \approx A\rho_{xx}^2(T,B)$ with $A \approx$ const was found. This corresponds to a Hall conductivity $\sigma_{xy} \approx -A$ that is constant in the relevant temperature and magnetic-field range. Indeed, a magnetic-field-independent Hall conductivity is expected in the mixed state within the Bardeen-Stephen model. In Fig. 22 we have plotted $\sigma_{xy}(B)$ for our NCCO thin films. The data correspond to the magnetic-field range with $\rho_{xx}(B) \geqslant 0.1\rho_n$ for the underdoped sample and $\rho_{xx}(B) \geqslant 0.2\rho_n$ for the optimally doped and the overdoped sample. In case of the underdoped sample a linear behavior of $\sigma_{xy}(B)$ can be observed over the entire magnetic-field range whereas deviations from this behavior increase with progressive doping. Therefore, the dominance of the normal-state contribution to σ_{xy} for the underdoped sample is possibly caused by the two-dimensional nature and the resulting pronounced fluctuation effects. Again, this might be regarded as an indication for the importance of the dimensionality for the resistive transition of these materials. However, we do not have a detailed understanding of the Hall effect in the mixed state of NCCO. Here, we have not discussed the influence of pinning (which is expected to increase if we change from a 2D to a 3D system), since it has been argued that pinning in general does not affect the Hall conductivity in the mixed state of type-II superconductors.[32]

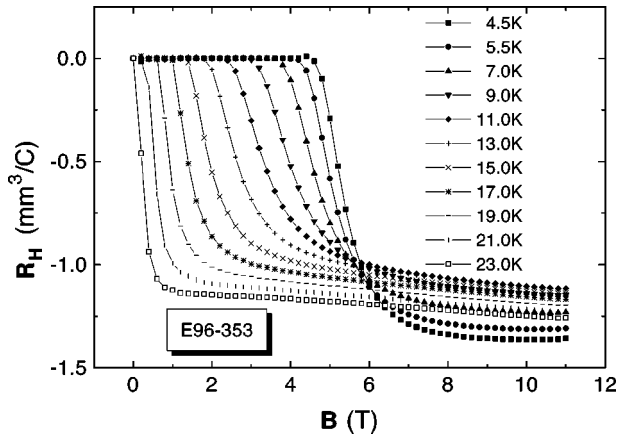

FIG. 21. Magnetic-field dependence of the Hall coefficient R_H for the optimally doped sample.

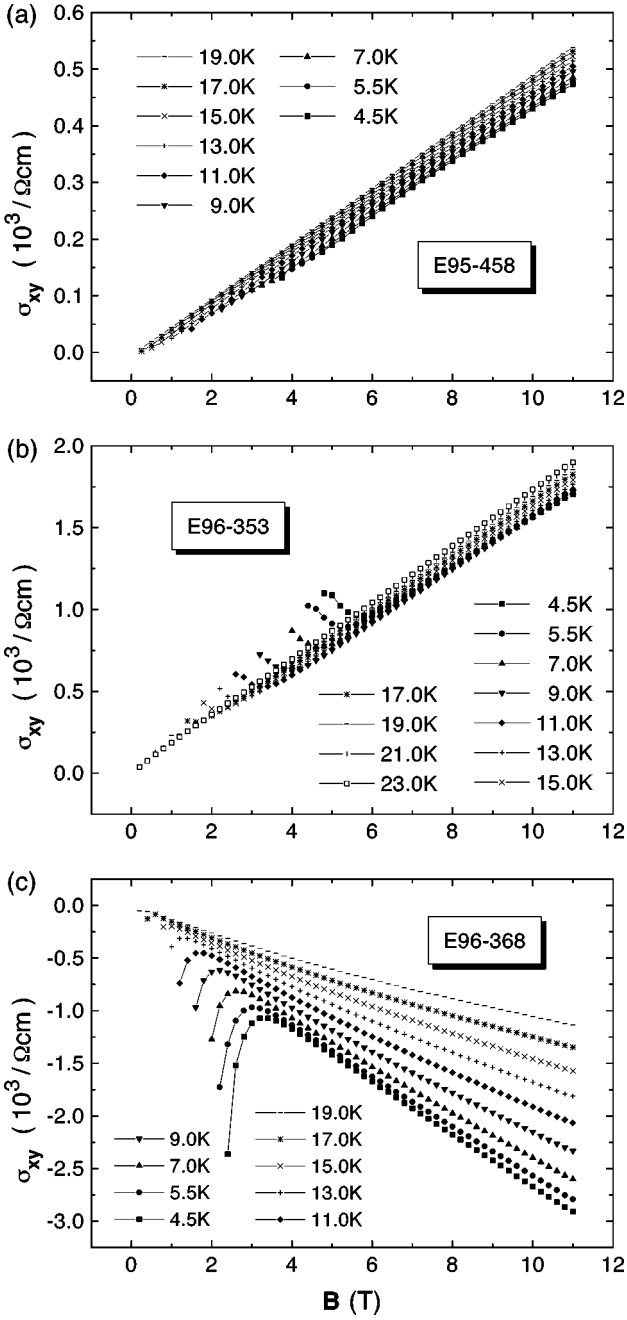

FIG. 22. Hall conductivities $\sigma_{xy}(B)$ for the three NCCO samples in the order of increasing doping. Note that $\sigma_{xy} = -\rho_{xy}/(\rho_{xx}^2 + \rho_{xy}^2)$.

VI. SUMMARY

We have studied the electric and thermomagnetic transport properties of an underdoped, an optimally doped, and an overdoped c-axis oriented, epitaxial NCCO thin film in the normal as well as in the superconducting state. In the normal state, the electric transport coefficients ρ, R_H, and $\Delta\rho/\rho(B)$ can be well described within a simple two-carrier model, where each of the two groups of charge carriers is characterized by a T-independent Hall coefficient. The derived transport coefficients of the isolated bands exhibit systematic dop-

ing dependences. Based on an analysis for a 2D metal with tetragonal symmetry within standard Boltzmann theory, the two-band model was extended to the thermomagnetic effects. This model does not result in a satisfactory description of the experimental data. Obviously, the relaxation-time approximation does not provide a good basis for an understanding of the thermomagnetic effects. Phonon-drag effects probably have to be taken into account. Nevertheless, the normal-state transport properties of NCCO possibly can be understood within a two-band model. An open question remains the physical origin of the two conduction bands.

In the superconducting regime, the critical field $B_\rho^*(T)$, derived from the shift of the resistive transition in external magnetic fields, displays a positive curvature. B_ρ^* is not identical with the upper critical field B_{c2} that results from an analysis of the fluctuation conductivity and the vortex transport entropy. Extrapolation to low temperatures suggests that $B_\rho^*(T=0)=B_{c2}(T=0)$. The quasi-two-dimensional nature of the single-layer cuprate NCCO seems to be responsible for the discrepancy between B_ρ^* and B_{c2}. Finally, the order of magnitude of the vortex transport entropy S_ϕ is consistent with predictions of the GL theory. Our results therefore suggest that the superconducting transport properties of NCCO also might be understood within classical concepts if the layered structure of this material is taken into account.

ACKNOWLEDGMENTS

One of the authors (F.G.) would like to thank R. P. Huebener and N. Schopohl for many helpful discussions and critically reading the manuscript.

[1] H. Takagi, S. Uchida, and Y. Tokura, Phys. Rev. Lett. **62**, 1197 (1989).
[2] Y. Tokura, H. Takagi, and S. Uchida, Nature (London) **337**, 345 (1989).
[3] S. M. Anlage, D.-H. Wu, J. Mao, S. N. Mao, X. X. Xi, T. Venkatesan, J. L. Peng, and R. L. Greene, Phys. Rev. B **50**, 523 (1994).
[4] C. W. Schneider, Z. H. Barber, J. E. Evetts, S. N. Mao, X. X. Xi, and T. Venkatesan, Physica C **233**, 77 (1994).
[5] D. M. King, Z.-X. Shen, D. S. Dessau, B. O. Wells, W. E. Spicer, A. J. Arko, D. S. Marshall, J. DiCarlo, A. G. Loeser, C. H. Park, E. R. Ratner, J. L. Peng, Z. Y. Li, and R. L. Greene, Phys. Rev. Lett. **70**, 3159 (1993).
[6] W. Jiang, S. N. Mao, X. X. Xi, X. Jiang, J. L. Peng, T. Venkatesan, C. J. Lobb, and R. L. Greene, Phys. Rev. Lett. **73**, 1291 (1994).
[7] S. N. Mao, W. Jiang, X. X. Xi, Q. Li, J. L. Peng, R. L. Greene, T. Venkatesan, D. Prasad Beesabathina, L. Salamanca-Riba, and X. D. Wu, Appl. Phys. Lett. **66**, 2137 (1995).
[8] M. Naito, H. Sato, and H. Yamamoto, Physica C **293**, 36 (1997).
[9] M. Naito and H. Sato, Appl. Phys. Lett. **67**, 2557 (1995).
[10] H.-C. Ri, R. Gross, F. Gollnik, A. Beck, R. P. Huebener, P. Wagner, and H. Adrian, Phys. Rev. B **50**, 3312 (1994).
[11] F. Gollnik, doctor thesis, Tübingen, 1997.
[12] H. H. Sample, B. L. Brandt, and L. G. Rubin, Rev. Sci. Instrum. **53**, 1129 (1982).
[13] B. L. Brandt, L. G. Rubin, and H. H. Sample, Rev. Sci. Instrum. **59**, 642 (1988).
[14] R. B. Roberts, Nature (London) **265**, 226 (1997); Philos. Mag. **36**, 91 (1977).
[15] R. S. Crisp, W. G. Henry, and P. A. Schroeder, Philos. Mag. **10**, 553 (1964).
[16] Z. Z. Wang, T. R. Chien, N. P. Ong, J. M. Tarascon, and E. Wang, Phys. Rev. B **43**, 3020 (1991).
[17] M. A. Crusellas, J. Fontcuberta, S. Puñol, M. Cagigal, and J. L. Vicent, Physica C **210**, 221 (1993).
[18] P. Fournier, X. Jiang, W. Jiang, S. N. Mao, T. Venkatesan, C. J. Lobb, and R. L. Greene, Phys. Rev. B **56**, 14 149 (1997).
[19] R. O. Anderson, R. Claessen, J. W. Allen, C. G. Olson, C. Janowitz, L. Z. Liu, J.-H. Park, M. B. Maple, Y. Dalichaouch, M. C. de Andrade, R. F. Jardim, E. A. Early, S.-J. Oh, and W. P. Ellis, Phys. Rev. Lett. **70**, 3163 (1993).
[20] S. Massidda, N. Hamada, J. Yu, and A. J. Freeman, Physica C **157**, 571 (1989).
[21] J. M. Harris, Y. F. Yan, P. Matl, N. P. Ong, P. W. Anderson, T. Kimura, and K. Kitazawa, Phys. Rev. Lett. **75**, 1391 (1995).
[22] Frank J. Blatt, *Physics of Electronic Conduction in Solids* (McGraw-Hill, New York, 1968).
[23] $(-\partial f_0/\partial\epsilon)$ has the character of a δ distribution:
$$\int F(\epsilon)\left(-\frac{\partial f_0}{\partial\epsilon}(\epsilon)\right)d\epsilon=F(\mu)+\frac{\pi^2}{6}(k_BT)^2\frac{d^2F}{d\epsilon^2}(\mu)+\cdots.$$
[24] J. A. Clayhold, Phys. Rev. B **54**, 6103 (1996).
[25] C. C. Tsuei, A. Gupta, and G. Koren, Physica C **161**, 415 (1989).
[26] J. L. Cohn, S. A. Wolf, V. Selvamanickam, and K. Salama, Phys. Rev. Lett. **66**, 1098 (1991).
[27] W. Jiang, X. Q. Xu, S. J. Hagen, J. L. Peng, Z. Y. Li, and R. L. Greene, Phys. Rev. B **48**, 657 (1993).
[28] M. Brinkmann, T. Rex, H. Bach, and K. Westerholt, Phys. Rev. Lett. **74**, 4927 (1995).
[29] S. Ullah and A. T. Dorsey, Phys. Rev. Lett. **65**, 2066 (1990).
[30] S. Ullah and A. T. Dorsey, Phys. Rev. B **44**, 262 (1991).
[31] M. B. Salamon and J. Shi, Phys. Rev. Lett. **69**, 1622 (1992).
[32] V. M. Vinokur, V. B. Geshkenbein, M. V. Feigel'mann, and G. Blatter, Phys. Rev. Lett. **71**, 1242 (1993).
[33] K. Maki, J. Low Temp. Phys. **1**, 45 (1969).
[34] C.-R. Hu, Phys. Rev. B **14**, 4834 (1976).
[35] K. Maki, Physica (Utrecht) **555**, 124 (1971).
[36] Z. Hao and J. R. Clem, Phys. Rev. B **43**, 2844 (1991).
[37] Z. Hao and J. R. Clem, Phys. Rev. Lett. **67**, 2371 (1991).
[38] Y. Hidaka and M. Suzuki, Nature (London) **338**, 635 (1989).
[39] Y. Dalichaouch, B. W. Lee, C. L. Seaman, J. T. Markert, and M. B. Maple, Phys. Rev. Lett. **64**, 599 (1990).
[40] A. P. Mackenzie, S. R. Julian, G. G. Lonzarich, A. Carrington, S. D. Hughes, R. S. Liu, and D. C. Sinclair, Phys. Rev. Lett. **71**, 1238 (1993).
[41] M. S. Osofsky, R. J. Soulen, Jr., S. A. Wolf, J. M. Broto, H. Rakoto, J. C. Ousset, G. Coffe, S. Askenazy, P. Pari, I. Bozovic, J. N. Eckstein, and G. F. Virshup, Phys. Rev. Lett. **71**, 2315 (1993).
[42] Y. N. Ovchinnikov and V. Z. Kresin, Phys. Rev. B **54**, 1251 (1996).

[43] A. Carrington, A. P. Mackenzie, and A. Tyler, Phys. Rev. B **54**, 3788 (1996).
[44] S. H. Han, C. C. Almasan, M. C. de Andrade, Y. Dalichaouch, and M. B. Maple, Phys. Rev. B **46**, 14 290 (1992).
[45] J. Herrmann, M. C. de Andrade, C. C. Almasan, R. P. Dickey, M. B. Maple, W. Jiang, S. N. Mao, and R. L. Greene, Phys. Rev. B **54**, 3610 (1996).
[46] N. R. Werthamer, E. Helfand, and P. C. Hohenberg, Phys. Rev. **147**, 295 (1966); **147**, 288 (1966).
[47] V. G. Kogan, A. Gurevich, J. H. Cho, D. C. Johnston, M. Xu, J. R. Thompson, and A. Martynovich, Phys. Rev. B **54**, 12 386 (1996).
[48] X. Jiang, W. Jiang, S. N. Mao, R. L. Greene, T. Venkatesan, and C. J. Lobb, Physica C **254**, 175 (1995).
[49] J. A. Clayhold, Y. Y. Xue, C. W. Chu, J. N. Eckstein, and I. Bozovic, Phys. Rev. B **53**, 8681 (1996).
[50] Y. Sato, I. Terasaki, and S. Tajima, Phys. Rev. B **54**, 6676 (1996).
[51] M. Houssa, M. Ausloos, and M. Pekala, Phys. Rev. B **54**, 12 713 (1996).
[52] F. Gollnik and R. P. Huebener, Phys. Rev. B **57**, 7495 (1998).